high diffusibility (e.g., in solution) (k) according to Eq. (1), as described by Karel and Saguy (28)

$$k' = k\left(\frac{1}{1+\frac{k}{\alpha D_r}}\right) = k\left(\frac{\alpha D_r}{k+\alpha D_r}\right) \quad (1)$$

where D_r is diffusion coefficient of the reactant and α is a constant representing the correlation between D_r and reaction rate. When αD is much larger than k ($\alpha D_r \gg k$), the value in the parentheses equals to unit, conforming k′ to k. As D_r decreases, the value in the parentheses decreases, making k′ smaller than k. As clearly shown by Eq. (1), the constant α corresponds to the slope of the k′ *vs.* D_r plot when αD is much smaller than *k* ($\alpha D_r \ll k$). The value of α may depend on the degradation mechanism, that is, whether the degradation involves translational or rotational motions of entire molecules, or intramolecular motions of specific portions of the molecule.

D_r in Eq. (1) can be estimated (4) from structural relaxation time (τ) according to Eq. (2):

$$\frac{D_{r2}}{D_{r1}} \approx \left(\frac{T_2}{T_1}\right)\left(\frac{\tau_1}{\tau_2}\right)^{\xi} \quad (2)$$

where ξ is a constant that represents the degree of decoupling between D_r and τ. τ can be calculated from T_g and fragility parameter (m) using the Vogel-Tammann-Fulcher (VTF) (29) and Adam-Gibbs-Vogel (AGV) (30) equations [Eqs. (3) and (4)] above and below the T_g, respectively.

$$\tau(T) = \tau_0 \exp\left(\frac{DT_0}{T-T_0}\right) \quad (3)$$

$$\tau(T,T_f) = \tau_0 \exp\left(\frac{DT_0}{T-(T/T_f)T_0}\right) \quad (4)$$

where τ_0 is the relaxation time at the high temperature limit (10^{-14} s), T_f is fictive temperature (approximated by T_g for newly formed glasses), $D = 2.303(m_{min})^2/(m - m_{min})$, $T_0 = T_g(1 - m_{min}/m)$, and $m_{min} = \log(\tau_{T_g}/\tau_0)$.

On the other hand, k in Eq. (1) can be related to the activation energy (ΔH) and frequency factor (A) according to Eq. (5):

$$k = A \exp\left(\frac{-\Delta H}{RT}\right) \quad (5)$$

where R is the gas constant. Therefore, Eq. (1) can be written as Eq. (6), by substituting Eq. (2) for D_r and Eq. (5) for k. k′ in Eq. (6) can be converted to t_{90} (the time required for 10% degradation), which is convenient for comparing with relaxation time. Thus, the dependence of t_{90} on factors reflecting the activational barrier (ΔH and A) and factors reflecting the molecular mobility (T_g, m, and α) can be described by Eq. (6), which allows quantitative assessment of the significance of molecular mobility as a determinant of t_{90}.

$$k' = \frac{A \exp\left(\frac{-\Delta H}{RT}\right)\alpha T\left(\frac{1}{\tau}\right)^{\xi}}{A \exp\left(\frac{-\Delta H}{RT}\right)+\alpha T\left(\frac{1}{\tau}\right)^{\xi}} = \frac{-\ln(0.9)}{t_{90}} \quad (6)$$

To assess the effects of T_g, ΔH, and α on the temperature dependence of t_{90}, simulations based on Eq. (6), using representative values for various parameters, were carried out. The results are shown in Fig. 4, where A and m were assumed to be 10^{14} s^{-1} and 70, respectively. Figure 4A shows the temperature dependence of t_{90} calculated using Eq. (6) as a function of T_g, assuming that ΔH is equal to 30 kcal/mol and α is 10^{-8}. Differences in water content change the T_g, and as

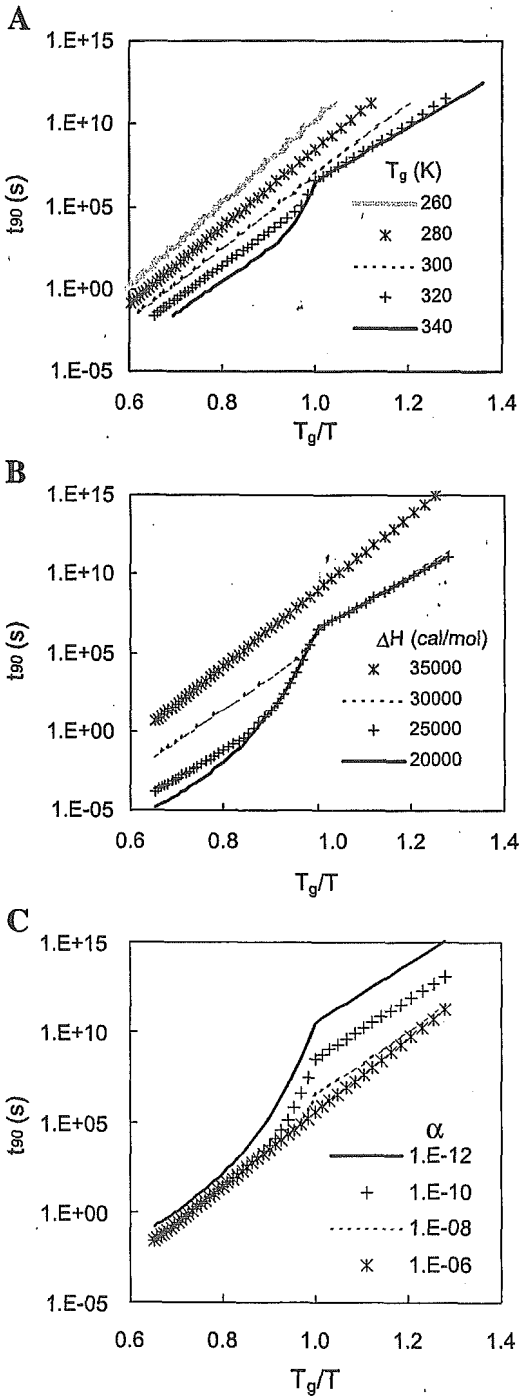

Fig. 4. Effect of T_g, ΔH, and α on the temperature dependence of t_{90} calculated according to Eq. (6) (m = 70). (A) t_{90} as a function of T_g (K) when ΔH = 30 kcal/mol and $\alpha = 10^{-8}$. (B) t_{90} as a function of ΔH when T_g = 320 K and $\alpha = 10^{-8}$. (C) t_{90} as a function of α when T_g = 320 K and ΔH = 30 kcal/mol.

a consequence bring about changes in the shape of temperature dependence for t_{90}, as shown in Fig. 4A, in which ΔH and α are assumed to be not affected by differing water contents. As T_g decreases (molecular mobility increases), the contribution of αD_r to k′ in Eq. (1) decreases because of a larger value of αD_r compared to k. Thus, k′ is determined by k to a larger extent, resulting in a smaller change in the slope of the temperature dependence occurring around T_g.

Figure 4B shows the temperature dependence of t_{90} as a function of ΔH, assuming that T_g is equal to 320 K, and α is 10^{-8}. As ΔH increases, the contribution of αD_r to k′ decreases because of a smaller value of k compared to αD_r, resulting in a smaller change in the slope of the temperature dependence occurring around T_g.

Figure 4C shows the temperature dependence of t_{90} as a function of α, assuming that T_g equals 320 K, and ΔH is 30 kcal/mol. As α increases, the contribution of αD_r to k′ decreases, resulting in a smaller change in the slope of temperature dependence occurring around T_g.

As shown in Fig. 4A, increases in T_g increase the contribution of molecular mobility to k′. To compare the contribution of molecular mobility with that of the activational barrier, k′/k was calculated for the model reaction shown in Fig. 4A, and the results are shown in Fig. 5. When T_g is low (280 K), the contribution of the activational barrier is predominant regardless of temperature. In contrast, when T_g is high (340, 320, or 300 K), the contribution of the activational barrier is predominant at lower T_g/T (higher temperature), and it decreases substantially with decreasing temperature (approaching T_g). This is because the slope of temperature dependence for the τ calculated by the VTF equation is larger than ΔH (30 kcal/mol) at temperatures near the T_g. When temperature decreases below the T_g, the slope of the k′/k *vs.* T_g/T curve becomes positive, because ΔH is larger than the slope of temperature dependence for the τ calculated by the AGV equation. Equation (6) can be applied only for reactions that exhibit an activation energy independent of temperature.

Significance of Molecular Mobility as a Determinant of t_{90} for Insulin Degradation and Dimerization

Figure 6 shows the $t_{90} - T_g/T$ plots for insulin degradation and dimerization in trehalose and PVP formulations

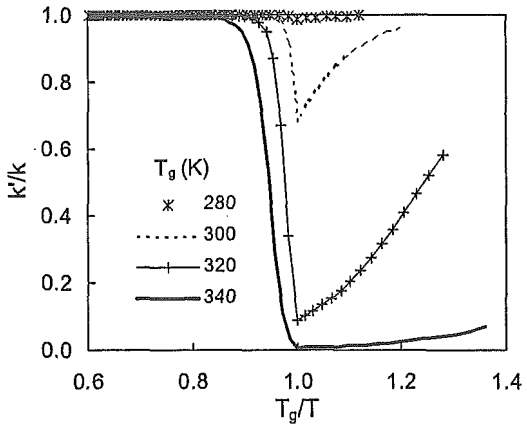

Fig. 5. Contribution of activational barrier to the t_{90} shown in Fig. 4A.

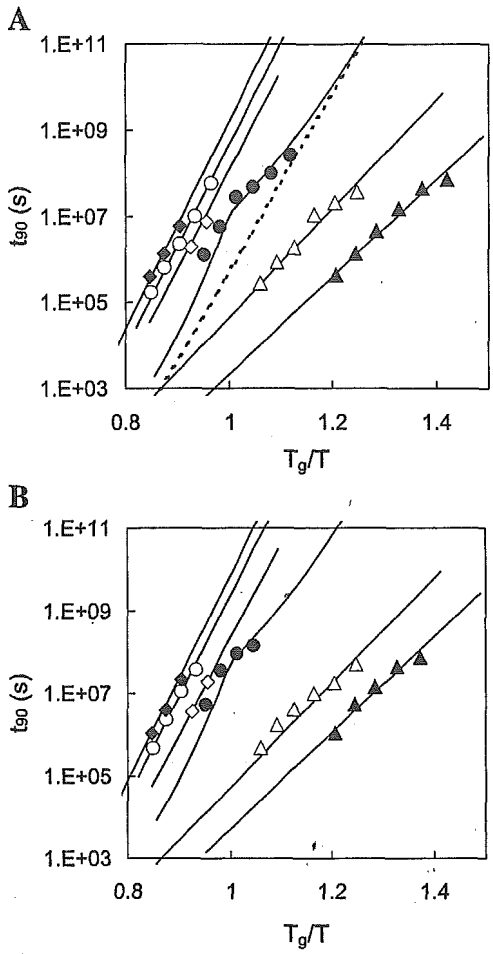

Fig. 6. Temperature dependence of t_{90} for insulin degradation (A) and dimerization (B). (●) trehalose 12% RH; (◇) trehalose 23% RH; (○) trehalose 33% RH; (◆) trehalose 43% RH; (▲) PVP 12% RH; (△) PVP 43% RH. Solid line for the t_{90} observed at 12% RH in insulin–trehalose formulation represents the least-squared regression curve according to Eq. (6), and dotted line represents the t_{90} calculated from k. Lines for other conditions represent the least-squared regression curve according to Eq. (5).

with differing T_g values attributable to differing water contents. Comparison of the $t_{90} - T_g/T$ plots for insulin degradation (Fig. 6A) with the simulated plots shown in Fig. 4A indicates that t_{90} for insulin degradation at 12% RH in the trehalose formulation is affected by the molecular mobility of the matrix. Curve-fitting of the observed t_{90} to Eq. (6), assuming τ_0 of 10^{-14} s, A of 10^{14} s^{-1}, m of 45 (calculated from the width of the glass transition measured by DSC) and ξ of 0.75, provided a ΔH estimate of 30.0 kcal/mol and an α estimate of 1×10^{-9}. The ξ value of 0.75, which is considered to be the lower limit of ξ representing the degree of decoupling between τ and D_r (31), gave a best fit. The dotted line in Fig. 6A represents the temperature dependence of t_{90} calculated from k, namely t_{90} determined by the activational barrier. The value of k′/k was calculated to be 0.051 at the T_g, indicating that the reaction rate is determined predominantly by the molecular mobility of the matrix. Thus, the observed t_{90} for insulin degradation at 12% RH appears to correspond to the simulated case with a high T_g value shown in Figs. 4A and 5.

For the trehalose formulations with lower T_g values, a linear temperature dependence was observed at temperatures above T_g, giving a ΔH estimate of 31.5, 30.8, and 30.4 kcal/mol for 23% RH, 33% RH, and 43% RH, respectively. The values of k'/k at T_g, calculated from the ΔH estimate and the t_{90} value at T_g obtained by extrapolation of the observed values, were 0.914, 0.978, and 0.994 for 23% RH, 33% RH, and 43% RH, respectively. These findings suggest that the reaction rate is determined predominantly by the activational barrier, and molecular mobility is sufficiently high such that molecular mobility is not involved in the rate-determining step. Thus, the t_{90} for insulin degradation under these conditions appears to correspond to the simulated case with a low T_g value shown in Figs. 4A and 5.

The t_{90} for insulin degradation in the trehalose formulations observed at temperatures above T_g was normalized against the t_{90} at T_g, and plotted against T_g/T in Fig. 7 in comparison with the structural relaxation time (τ) calculated according to the VTF equation from the values of T_g and m measured by DSC. This normalized $t_{90} - T_g/T$ plot exhibited a linear relationship with a smaller slope than the τ calculated using a ξ value of 0.75. This finding supports the thought that the contribution of molecular mobility to the reaction rate is negligible under these conditions.

For insulin degradation in the trehalose formulation, it may be concluded that differences in water content do not bring about significant differences in ΔH, but rather differences in the contribution of molecular mobility to the degradation rate.

For insulin degradation in the PVP formulation, it cannot be judged whether the slope of the $t_{90} - T_g/T$ plot changes around the T_g, because of the lack of data at temperatures above T_g (Fig. 6A). The slope below T_g was close to that observed for the trehalose formulation with the highest T_g value, and smaller than those observed in the trehalose formulations with lower T_g values, the t_{90} of which is determined predominantly by the activational barrier. However, the value of t_{90} at T_g (extrapolated from observed values) exhibited a large difference between the PVP formulations with differing T_g values because of differing water contents, indicating that the molecular mobility of the matrix is not involved in the rate-determining step. Insulin degradation under these conditions appears to correspond to the simulated case in which t_{90} is determined by the activational barrier shown in Fig. 4A. Curve fitting to Eq. (6) provided estimates of A of 10^7 s^{-1} as well as ΔH of 20.8 and 20.4 kcal/mol for 12% RH and 42% RH, respectively.

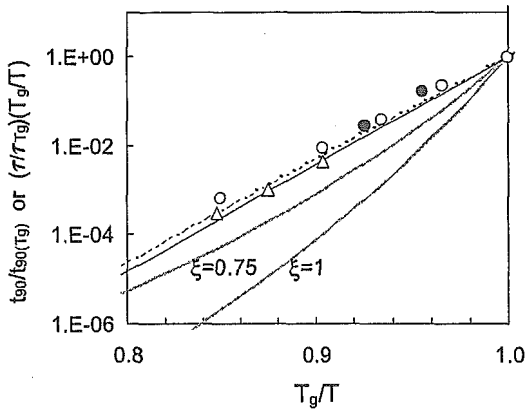

Fig. 7. Temperature dependence of the normalized t_{90} for insulin degradation in the trehalose formulation obtained above T_g [(●) 23%RH, (○) 33% RH, (△) 43% RH] fitted to the Arrhenius equation (dotted and solid lines represent regression curves for t_{90} at 23% RH and 43% RH, respectively, calculated using each ΔH estimate and a common A value of 10^{14} s^{-1}). t_{90} is compared to the structural relaxation time calculated according to the VTF equation using an m value of 50 and ξ values of 1 and 0.75 (——).

The T_g dependence of t_{90} for the PVP formulation is compared with the structural relaxation time calculated according to the AGV equation using a ξ value of 0.75 in Fig. 3. The slope of the $t_{90} - T_g/T$ plot for the data obtained at a constant temperature but at different humidities was much smaller than that for the structural relaxation time, supporting the thought that the contribution of molecular mobility to the degradation rate is negligible. However, the slope of the $t_{90} - T_g/T$ plot should be zero without the effect of molecular mobility, if A and ΔH are independent of humidity (water content). The observed positive slope suggests that a difference in water content brings about a small difference in ΔH. This idea is supported by the ΔH values obtained by curve-fitting (Fig. 6A), which tended to increase slightly with decreasing water content.

Insulin dimerization in the trehalose and PVP formulations exhibited temperature dependence similar to that of insulin degradation, as shown in Fig. 6B. The contribution of molecular mobility to the t_{90} appeared to be small, except for the t_{90} observed at 12% RH in the trehalose formulation. Curve-fitting to Eq. (6) gave slightly greater values of ΔH compared with those for insulin degradation both for the trehalose (31.8, 31.5, and 31.1 kcal/mol for 23% RH, 33% RH, and 43% RH, respectively) and PVP formulations (21.5 and 20.5 kcal/mol for 12% RH and 43% RH).

Significant differences were observed in insulin degradation and dimerization behaviors between the trehalose and PVP formulations. The reactivity of insulin in the trehalose formulation was much smaller than that in the PVP formulation, when compared at the same T_g/T (namely same molecular mobility of the matrix), as shown in Fig. 3. A and ΔH were estimated to be 10^{14} s^{-1} and approximately 30 kcal/mol, respectively, for the trehalose formulation, compared with 10^7 s^{-1} and approximately 20 kcal/mol for the PVP formulation. These findings suggest that reaction mechanisms are different between the two formulations. The much smaller value of A obtained for the PVP formulation may indicate a reaction mechanism other than a simple monomolecular reaction. One other possible explanation for these differences may be qualitative and quantitative differences in insulin-excipient interaction behavior or in phase separation behavior. In addition, PVP may react with insulin to produce a PVP–insulin adduct in a similar manner as was observed for a PVP–hexapeptide adduct (32). Further studies are required to interpret the differences in the reactivity between the trehalose and PVP formulations. In addition, the relationship between the matrix mobility described in the present article and the local mobility of reactants such as polymer side chains and water molecules needs to be elucidated in order to discuss the effect of molecular mobility based on the degradation mechanism.

CONCLUSION

The reactivity of insulin in the trehalose and PVP formulations can be described by Eq. (6) including factors reflecting the activational barrier (ΔH and A) and factors reflecting the molecular mobility (T_g, m, and α). Thus, analysis of temperature dependence based on Eq. (6) allows quantitative assessment of the significance of molecular mobility as a determinant of chemical reactivity.

ACKNOWLEDGMENT

The authors would like to thank Prof. G. Zografi of the University of Wisconsin-Madison for his valuable comments and encouragement during the preparation of this manuscript.

REFERENCES

1. S. P. Duddu and K. Weller. Importance of glass transition temperature in accelerated stability testing of amorphous solids: case study using a lyophilized aspirin formulation. *J. Pharm. Sci.* **85**:345–347 (1996).
2. L. Streefland, A. D. Auffret, and F. Franks. Bond cleavage reactions in solid aqueous carbohydrate solutions. *Pharm. Res.* **15**:843–849 (1998).
3. M. C. Lai, M. J. Hageman, R. L. Schowen, R. T. Borchardt, and E. M. Topp. Chemical stability of peptides in polymers. 2. Discriminating between solvent and plasticizing effects of water on peptide deamidation in poly(vinylpyrrolidone). *J. Pharm. Sci.* **88**:1081–1089 (1999).
4. Y. Guo, S. R. Byrn, and G. Zografi. Physical characteristics and chemical degradation of amorphous quinapril hydrochloride. *J. Pharm. Sci.* **89**:128–143 (2000).
5. J. Li, Y. Guo, and G. Zografi. The solid-state stability of amorphous quinapril in the presence of β-cyclodextrins. *J. Pharm. Sci.* **91**:229–243 (2002).
6. S. Yoshioka, Y. Aso, and S. Kojima. Temperature dependence of bimolecular reactions associated with molecular mobility in lyophilized formulations. *Pharm. Res.* **17**:925–929 (2000).
7. S. Yoshioka, Y. Aso, and S. Kojima. Temperature- and glass transition temperature-dependence of bimolecular reaction rates in lyophilized formulations described by the Adam-Gibbs-Vogel equation. *J. Pharm. Sci.* **93**:1062–1069 (2004).
8. V. Andronis, M. Yoshioka, and G. Zografi. Effect of sorbed water on the crystallization of indomethacin from the amorphous state. *J. Pharm. Sci.* **86**:346–351 (1997).
9. V. Andronis and G. Zografi. Crystal nucleation and growth of indomethacin polymorphs from the amorphous state. *J. Non-Cryst. Solids* **271**:236–248 (2000).
10. Y. Aso, S. Yoshioka, and S. Kojima. Explanation of the crystallization rate of amorphous nifedipine and phenobarbital from their molecular mobility as measured by ^{13}C nuclear magnetic resonance relaxation time and the relaxation time obtained from the heating rate dependence of the glass transition temperature. *J. Pharm. Sci.* **90**:798–806 (2001).
11. D. Zhou, G. G. Z. Zhang, D. Law, D. J. W. Grant, and E. A. Schmitt. Physical stability of amorphous pharmaceuticals: importance of configurational thermodynamic quantities and molecular mobility. *J. Pharm. Sci.* **91**:1863–1872 (2002).
12. Y. Aso, S. Yoshioka, and S. Kojima. Molecular mobility-based prediction of the crystallization rate of amorphous nifedipine and phenobarbital in PVP solid dispersions of the paracetamol amorphous form. *J. Pharm. Sci.* **93**:384–391 (2004).
13. S. P. Duddu, G. Zhang, and P. R. Dal Monte. The relationship between protein aggregation and molecular mobility below the glass transition temperature of lyophilized formulations containing a monoclonal antibody. *Pharm. Res.* **14**:596–600 (1997).
14. R. G. Strickley and B. D. Anderson. Solid-state stability of human insulin II. Effect of water on reactive intermediate partitioning in lyophiles from pH 2–5 solutions: stabilization against covalent dimer formation. *J. Pharm. Sci.* **86**:645–653 (1997).
15. S. Yoshioka, Y. Aso, and S. Kojima. Dependence of the molecular mobility and protein stability of freeze-dried γ-globulin formulations on the molecular weight of dextran. *Pharm. Res.* **14**:736–741 (1997).
16. S. Yoshioka, Y. Aso, Y. Nakai, and S. Kojima. Effect of high molecular mobility of poly(vinyl alcohol) on protein stability of lyophilized γ-globulin formulations. *J. Pharm. Sci.* **87**:147–151 (1998).
17. S. D. Allison, M. C. Manning, T. R. Randolph, K. Middleton, A. Davis, and J. F. Carpenter. Optimization of storage stability of lyophilized actin using combinations of disaccharides and dextran. *J. Pharm. Sci.* **89**:199–214 (2000).
18. S. Yoshioka, Y. Aso, and S. Kojima. Usefulness of the Kohlrausch-Williams-Watts stretched exponential function to describe protein aggregation in lyophilized formulations and the temperature dependence near the glass transition temperature. *Pharm. Res.* **18**:256–260 (2001).
19. S. Yoshioka, S. Tajima, Y. Aso, and S. Kojima. Inactivation and aggregation of β-galactosidase in lyophilized formlation described by Kohlrausch-Williams-Watts stretched exponential function. *Pharm. Res.* **20**:1655–1660 (2003).
20. W. Garzon-Rodriguez, R. L. Koval, S. Chongprasert, S. Krishnan, T. W. Randolph, N. W. Warne, and J. F. Carpenter. Optimizing storage stability of lyophilized recombinant human interleukin-11 with disaccharide/hydroxyethyl starch mixtures. *J. Pharm. Sci.* **93**:684–696 (2004).
21. J. Brange, S. Havelund, and P. Hougaard. Chemical stability of insulin. 2. Formulation of higher molecular weight transformation products during storage of pharmaceutical preparations. *Pharm. Res.* **9**:727–734 (1992).
22. R. T. Darrington and B. D. Anderson. Effect of insulin concentration and self-association on the partitioning of its a-21 cyclic anhydride intermediate to desamido insulin and covalent dimer. *Pharm. Res.* **12**:1077–1084 (1995).
23. M. J. Pikal and D. R. Rigsbee. The stability of insulin in crystalline and amorphous solids: observation of greater stability for the amorphous form. *Pharm. Res.* **14**:1379–1387 (1997).
24. R. T. Darrington and B. D. Anderson. The role of intramolecular nucleophilic catalysis and the effects of self-association on the deamidation of human insulin at low pH. *Pharm. Res.* **11**:784–793 (1994).
25. C. T. Moynihan, S.-K. Lee, M. Tatsumisago, and T. Minami. Estimation of activation energies for structural relaxation and viscous flow from DTA and DSC experiments. *Thermochim. Acta* **280/281**:153–162 (1996).
26. K. J. Crowley and G. Zografi. The use of thermal methods for predicting glass-former fragility. *Thermochim. Acta* **380**:79–93 (2001).
27. R. G. Strickley and B. D. Anderson. Solid-state stability of human insulin I. Mechanism and the effect of water on the kinetics of degradation in lyophiles from pH 2–5 solutions. *Pharm. Res.* **13**:1142–1153 (1996).
28. M. Karel and I. Saguy. Effects of water on diffusion in food systems. *Adv. Exp. Med. Biol.* **302**:157–173 (1991).
29. R. Bohmer, K. L. Ngai, C. A. Angell, and D. J. Plazek. Nonexponential relaxations in strong and fragile glass formers. *J. Chem. Phys.* **99**:4201–4209 (1993).
30. I. M. Hodge. Enthalpy relaxation and recovery in amorphous materials. *J. Non-Cryst. Solids* **169**:211–266 (1994).
31. F. Fujara, B. Geil, H. Sillescu, and G. Fleischer. Translational and rotational diffusion in supercooled orthoterphenyl close to the glass transition. *Z. Phys. B Condens. Matter* **88**:195–204 (1992).
32. A. J. D'Souza, R. L. Schowen, R. T. Borchardt, J. S. Salsbury, E. J. Munson, and E. M. Topp. Reaction of a peptide with polyvinylpyrrolidone in the solid state. *J. Pharm. Sci.* **92**:585–593 (2003).

Effect of Freezing Rate on Physical Stability of Lyophilized Cationic Liposomes

Yukio Aso* and Sumie Yoshioka

National Institute of Health Sciences; 1–8–1 Kamiyoga, Setagaya, Tokyo 158–8501, Japan.
Received October 1, 2004; accepted December 8, 2004; published online December 16, 2004

Factors affecting the storage stability of lyophilized cationic liposomes were investigated using liposomes prepared with various excipients and by different freezing rates, either quick freezing (freezing by immersion into liquid nitrogen) or slow freezing (cooling to −50 °C at a rate of −10 °C/h). Increases in the particle size of cationic liposomes observed during freeze-drying were inhibited by the addition of sucrose, trehalose and sucrose–dextran mixtures (1 : 1 and 2 : 1 by weight). The storage instability of the formulations, as indicated by changes in particle size, was affected by their glass transition temperature (T_g). Addition of high-T_g excipients resulted in smaller increases in the particle size, indicating improvement of storage stability. The storage stability of cationic liposome formulations was also affected by freezing rate. Formulations prepared by slow freezing exhibited better stability. Longer shear relaxation times were observed for formulations prepared by slow freezing compared with those prepared by quick freezing. This indicates that formulations prepared by slow freezing have a lower matrix mobility, which may result in better storage stability. T_g or ^{1}H-NMR relaxation measurements could not detect differences in matrix mobility between formulations prepared by different freezing rates. Shear relaxation measurements seem to be a useful method for evaluating the storage stability of cationic liposome formulations.

Key words cationic liposome; stability; lyophilization; shear relaxation time; molecular mobility

Cationic lipid has attracted much attention as a non-viral DNA vector. Cationic liposome–DNA complex (lipoplex), however, is usually unstable in solution and forms aggregates during long-term storage at room temperature, resulting in the loss of its transfection ability.[1,2] Stability of lipoplex during freeze-drying and subsequent storage can be improved by lyophilization with lyoprotectants such as sucrose.[3—5] The stabilizing effect of these compounds on liposomes during lyophilization has been attributed to incorporation of liposomes into glass matrices and hydrogen bonding between the excipient and the polar head group of lipids.[6] Therefore, the storage stability of lyophilized cationic liposomes is expected to be improved by addition of excipients with higher glass transition temperature (T_g), which yield glass matrices with a lower molecular mobility.

It is also known that process parameters such as freezing rate affect the stability of lyophilized formulations. It has been reported that the amount of drug entrapped in lyophilized liposomes is higher for formulations prepared by slow freezing than for those prepared by quick freezing.[7] The effect of freezing rate depended on the lipid composition and was most pronounced for rigid liposomes. The storage stability of lyophilized tissue-type plasminogen activator was also affected by freezing rate.[8] Faster freezing caused a larger surface area of the freeze-dried cake, and the storage stability of the incorporated protein was proportional to the surface area of the freeze-dried cake.

This paper describes the effects of excipients with different T_g as well as the effect of freezing rate on the storage stability of lyophilized cationic liposomes. Changes in the particle size of cationic liposomes were determined as a measure of storage instability. ^{1}H-NMR relaxation time and shear relaxation time of the freeze-dried cakes were also determined. The storage stability of cationic liposomes is discussed in terms of the molecular mobility and visco-elastic property (matrix mobility) of the freeze-dried cakes.

Experimental

Materials *N*-[1-(2,3-Dioleoyloxy) propyl]-*N*,*N*,*N*-trimethyl-ammonium chloride (DOTAP), cholesterol, sucrose, trehalose and dextran were purchased from Sigma (St. Louis, MO, U.S.A.).

Preparation of Cationic Liposomes[3] DOTAP (250 mg) and cholesterol (125 mg) were dissolved in chloroform (about 5 ml). The chloroform was evaporated with a stream of nitrogen gas to make a thin film of the lipids. The film was further dried under vacuum for 1 h and hydrated in 50 ml of water. The lipid suspension was incubated at 50 °C for 10 min and extruded through polycarbonate membranes (Millipore, Billerica, MA, U.S.A.) with pore sizes of 0.6 and 0.2 μm, which were connected in series.

Preparation of Lyophilized Liposome Formulations Sucrose, trehalose and sucrose–dextran mixtures (1 : 1 or 2 : 1 by weight) were used as excipients for lyophilized liposome formulations. Equal volumes of excipient solution (10 w/w%) and liposome suspension were mixed. Aliquots (500 μl) of the mixture were frozen in polypropylene tubes by immersion into liquid nitrogen (quick freezing) or by cooling on the shelf of a freeze drier (Freezevac C-3; Tozai Tsusho, Tokyo) at a rate of −10 °C/h to −50 °C (slow freezing). Frozen samples were dried under a vacuum of approximately 5 Pa. The shelf temperature was maintained at −40 °C for 24 h, −20 °C for 16 h, 0 °C for 6 h, and then 20 °C for 6 h.

Stability Study of Lyophilized Cationic Liposomes The water content of the lyophilized formulations was adjusted by storage at 25 °C and 23% RH for 1 d. The samples were stored at 40 or 25 °C in a thermostatic chamber and withdrawn at appropriate intervals. The storage stability of liposomes was evaluated from changes in particle size. Particle size was determined at 25 °C by dynamic light scattering with a DLS-7000 system (Otsuka Electronics Co. Ltd., Osaka). The viscosity of the rehydrated liposome suspension, required for the calculation of particle size, was determined with a model AR-1000 rheometer (TA Instruments, Inc., New Castle, DE, U.S.A.). The T_g values of the formulations are summarized in Table 1.

Physicochemical Properties of Lyophilized Liposome Formulations. Determination of the Complex Shear Modulus The visco-elastic property (matrix mobility) of the freeze-dried cakes was examined with the model AR-1000 rheometer. A freeze-dried cake was placed on the sample platform of the instrument and compressed to about 440 μm thickness with a flat plate geometry (40 mm in diameter). An oscillating stress of 40 Pa was applied to the sample over a frequency range of 0.01 to 600 radian/s. The effect of sample size, which was smaller than the plate size of the geometry used, on the determination of shear relaxation time was considered to be negligible, since shear relaxation time was estimated from relative changes in the shear modulus determined as a function of stress frequency.

^{1}H-NMR Relaxation Measurements In order to determine the molecu-

* To whom correspondence should be addressed. e-mail: aso@nihs.go.jp

lar mobility of the freeze-dried cakes, spin–lattice relaxation times in laboratory frame (T_1) and rotating frame ($T_{1\rho}$) were measured at 27 °C with a model JNM-MU25 spectrometer (JEOL DATUM, Tokyo) operated at a ^{1}H resonance frequency of 25 MHz. A freeze-dried cake was placed in an NMR tube (10 mm outer diameter) and dried at 25 °C for 18 h under vacuum before measurement. T_1 was measured by the inversion-recovery method. A spin locking field of 1 mT was applied to the samples for $T_{1\rho}$ measurement.

DSC Analysis The T_g of freeze-dried cakes was determined with a model 2920 differential scanning calorimeter (TA Instruments, Inc.) equipped with a refrigerator cooling accessory. Temperature and heat flow calibration of the instrument was performed with indium. Approximately 3 mg of freeze-dried cake was weighed into a hermetic sample pan, which was stored at 25 °C and 23% RH for 24 h and then sealed. Samples were heated at a rate of 20 °C/min from −30 to 200 °C. The DSC cell was purged with nitrogen gas at 30 ml/min during measurement.

Water Vapor Sorption Measurements Time profiles of water vapor sorption for lyophilized liposome formulations containing sucrose and trehalose were measured at 25 °C and 10% RH with a GM-300 gravimetric sorption analyzer (VTI Corp., Hialeah, FL, U.S.A.). Approximately 25 mg of freeze-dried cake was placed in a sample holder and dried at 25 °C under vacuum. When no change in the weight of the cake was observed over 5 min, the cake was considered to be in a dry state. The cake was exposed to water vapor equivalent to 10% RH. The weight of the cake was measured at intervals of 30 s.

Results and Discussion

Effect of Excipients on Stability of Lyophilized Cationic Liposomes Figure 1 shows the effect of freeze-thaw and freeze-drying on the particle size of cationic liposomes. No significant difference in particle size was observed after the freeze-thaw cycle, regardless of the presence of excipients. Increases in the particle size, however, were observed after rehydration of liposomes lyophilized without excipient. On the other hand, liposomes lyophilized with excipients exhibited similar particle sizes before and after freeze-drying, indicating that all the excipients studied stabilized cationic liposomes against aggregation during drying.

Figure 2 shows the storage stability of cationic liposomes lyophilized with the excipients. Increases in particle size were observed during storage at 40 °C except for the trehalose formulation prepared by slow freezing. The liposome formulations containing sucrose, the T_g of which (32 °C) was lower than the storage temperature, were least stable. The formulations containing trehalose, the T_g of which (49 °C) was higher than the storage temperature, were more stable than the sucrose formulations. Addition of dextran to sucrose resulted in a higher T_g (43 °C for 2 : 1 sucrose–dextran mixture and 60 °C for 1 : 1 mixture) and increased the stability of the liposome formulations. These results indicate that the stability of cationic liposome formulations is closely correlated with the mobility of the formulation matrix as indicated by T_g. The formulation containing trehalose prepared by quick freezing exhibited increases in the particle size, but no significant increase was observed for the trehalose formulation prepared by slow freezing, indicating that the storage stability of lyophilized cationic liposomes is affected by the freezing rate.

Figure 3 shows a photograph of lyophilized cationic liposomes containing sucrose or trehalose stored at 25 °C and 23% RH for 1 year. Shrinkage of the freeze-dried cake was observed for sucrose formulations. The extent of shrinkage was larger for the sample prepared by quick freezing. No significant shrinkage of freeze-dried cakes was observed for trehalose formulations and sucrose–dextran formulations (data not shown), which had T_g values higher than those of sucrose formulations. Figure 4 shows the particle size of liposomes after storage at 25 °C and 23% RH for 1 year. The trehalose and sucrose–dextran formulations were stable, but an increase in the particle size was observed for sucrose formulations during storage at 25 °C (approximately 8 °C lower than the T_g of the sucrose formulation). These results indicate that the sucrose formulations have a sufficient degree of matrix mobility to cause liposome aggregation even at 25 °C, a temperature lower than the T_g of the formulation.

Molecular Mobility and Matrix Mobility of Cationic

Table 1. T_g of Lyophilized Cationic Liposome Formulations[a)]

Excipient	T_g (°C)[b)]	
	Slow freezing	Quick freezing
Sucrose	32.3	31.9
Trehalose	48.4	49.0
Suc–Dex (2 : 1)	43.5	43.7
Suc–Dex (1 : 1)	59.7	59.9

a) Water content was adjusted by storage at 25 °C and 23% RH for 1 d. *b*) T_g values reported were average of two determinations.

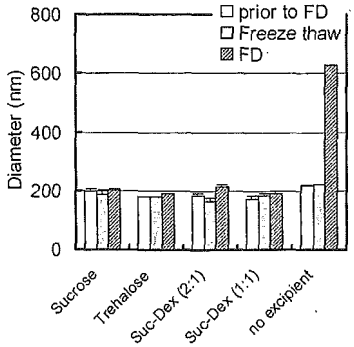

Fig. 1. Effect of Freeze-Thaw and Freeze-Drying on the Particle Size of Cationic Liposomes

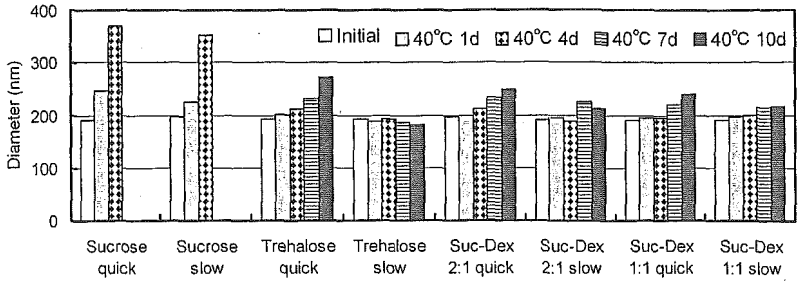

Fig. 2. Effect of Storage at 40 °C on the Particle Size of Cationic Liposomes

Liposome Formulations The storage stability of lyophilized cationic liposomes was affected by freezing rate, such that formulations prepared by quick cooling were less stable than those prepared by slow cooling, as shown in Figs. 2—4. To gain an insight into the mechanism of the effect of freezing rate on the stability of cationic liposome formulations, the mobility of the formulation matrices was examined by ^{1}H-NMR relaxation and shear relaxation measurements. Table 2 shows the T_1 and $T_{1\rho}$ of cationic liposome formulations. T_1 and $T_{1\rho}$ are measures of molecular mobility on time scales of the order of MHz and mid kHz, respectively.[9] T_1 and $T_{1\rho}$ of the formulations did not change with freezing rate within experimental error, indicating that freezing rate has little effect on the molecular mobility reflected in T_1 and $T_{1\rho}$.

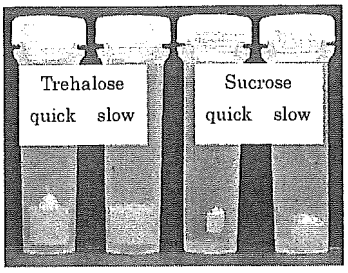

Fig. 3. Appearance of Freeze-Dried Cakes of Cationic Liposomes Containing Sucrose or Trehalose after Storage at 25 °C and 23% RH for 1 Year

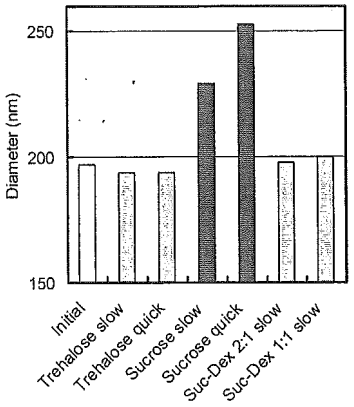

Fig. 4. Effect of Storage at 25 °C and 23% RH for 1 Year on Particle Size of Cationic Liposomes

Table 2. ^{1}H-NMR Relaxation Time of Cationic Liposome Formulations

Excipient		T_1 (s)	$T_{1\rho}$ (ms)
Sucrose	Slow	0.29	4.0
	Quick	0.28	4.0
Trehalose	Slow	0.28	4.4
	Quick	0.30	4.6

The mobility of formulation matrices on longer time scales than those reflected in NMR spin–lattice relaxation times was determined by measuring the frequency dependence of the shear modulus of lyophilized cationic liposomes (the visco-elastic property of the formulations). The frequency-dependent shear modulus ($G^*(\omega)$) of amorphous indomethacin has been shown to characterize the time scales of molecular motion of indomethacin in the amorphous state.[10] The storage modulus (G', a real part of $G^*(\omega)$) of visco-elastic materials increases with increasing frequency of shear stress, and the loss modulus (G'', an imaginary part of $G^*(\omega)$) exhibits a maximum. Visco-elastic materials behave as a viscous fluid and a rigid solid against low and high frequency stress, respectively. The shear relaxation time, the reciprocal of maximum frequency (in radian/s) of G'', can be used as a measure of mobility. Figure 5 shows the typical frequency dependence of the shear modulus of the cationic liposome formulation containing sucrose measured at 74 °C in the dry state. Figure 6 shows the temperature dependence of shear relaxation time for the cationic liposome formulations containing sucrose and trehalose measured under dry conditions. The relaxation time of the formulation prepared by slow freezing was longer than that of the formulation prepared by quick freezing. The effect of freezing rate on the shear relaxation time was also observed in the presence of moisture. Figure 7 shows the frequency dependence of G'' for the cationic liposome formulation containing sucrose stored at 25 °C and 23% RH for 1 d. The formulation prepared by

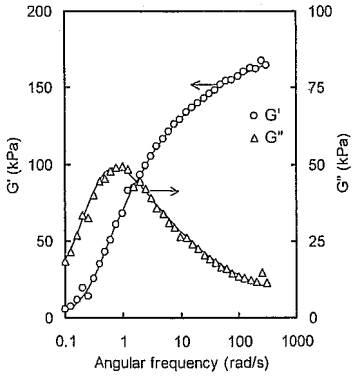

Fig. 5. Frequency Dependence of the Shear Modulus of a Cationic Liposome Formulation Containing Sucrose Measured at 74 °C in the Dry State

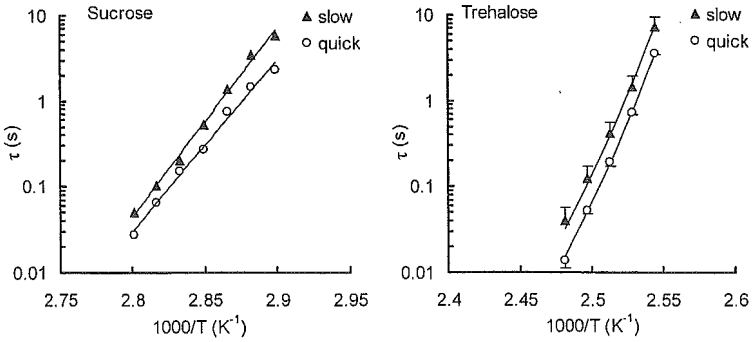

Fig. 6. Shear Relaxation Time of Cationic Liposome Formulations Measured under Dry Conditions

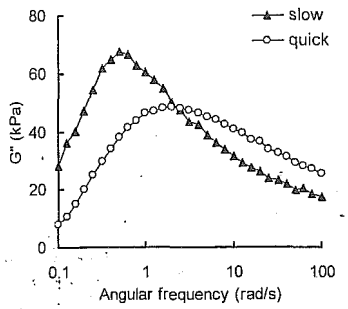

Fig. 7. Frequency Dependence of the Loss Modulus (G'') of a Cationic Liposome Formulation Containing Sucrose at 30 °C

The water content was adjusted by storage at 25 °C and 23% RH for 1 d.

quick freezing exhibited a maximum at 2 radian/s, whereas the formulation prepared by slow freezing exhibited a maximum at 0.4 radian/s. These results indicate that formulation matrices prepared by slow freezing have a lower mobility than those prepared by quick freezing. Temperature dependence of G'' supports this speculation. G'' at a frequency of 0.1 radian/s showed a maximum at 21 °C for the sucrose formulation prepared by quick freezing, whereas 26 °C for the sucrose formulation prepared by slow freezing. The maximum temperature corresponds to the temperature at which relaxation time of 10 s (inverse of 0.1 radian/s) is observed. Therefore, the relaxation time at 25 °C is considered to be longer than 10 s for the sucrose formulation prepared by slow freezing. In contrast, shorter relaxation time than 10 s is expected for the sucrose formulation prepared by quick freezing. This difference in matrix mobility resulting from different freezing rates may cause a difference in storage stability. The difference in matrix mobility of cationic liposome formulations prepared by different freezing rates could be detected by shear relaxation time, but not by T_g and ^{1}H-NMR relaxation measurements (Tables 1, 2). This finding suggests that the aggregation rate of lyophilized liposomes may correlate more closely with matrix mobility as measured by the shear relaxation time than with molecular mobility as measured by the spin-lattice relaxation time.

Figure 8 shows the time course of water vapor sorption for the cationic liposome formulations containing sucrose and trehalose stored at 25 °C and 10% RH. The water content at equilibrium was not affected by freezing rate. The weight of the formulations prepared by quick freezing, however, reached a plateau within 40 min, whereas it took more than 300 min to reach equilibrium for formulations prepared by slow freezing. The difference in water sorption rate indicates that the ratio of surface area to volume for the formulations prepared by quick freezing is larger than that for the formulations prepared by slow freezing. Similar differences in the surface area of freeze-dried cakes have been reported for lyophilized tissue-type plasminogen activator formulations.[8] Such dependence of the surface area on freezing rate may cause the different mobility of the formulation matrices, as indicated by the different shear relaxation times. Formulations with lager surface area may be more susceptive to changes in the T_g upon local temperature fluctuations and/or local humidity fluctuations. Differences in the susceptibility may affect the shrinkages of freeze-dried cakes and the stability of liposomes during storage.

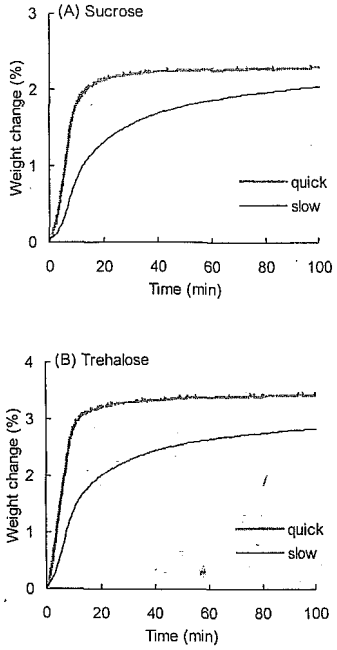

Fig. 8. Time Courses of Water Vapor Sorption of Cationic Liposome Formulations Stored at 25 °C and 10% RH

In conclusion, the storage instability of lyophilized cationic liposomes, as indicated by change in particle size, was affected by the T_g of the formulations. Formulations containing high-T_g excipients exhibited better storage stability. The storage stability of lyophilized cationic liposomes was also affected by freezing rate. Longer shear relaxation times were observed for formulations prepared by slow freezing compared with those prepared by quick freezing, indicating that formulations prepared by slow freezing have a lower matrix mobility. The lower matrix mobility of the formulations prepared by slow freezing may result in better storage stability. T_g or ^{1}H-NMR relaxation measurements could not detect these differences in matrix mobility. Shear relaxation measurements appear to be useful for evaluating the storage stability of cationic liposome formulations.

Acknowledgements A part of this work was supported by a Grant-in-aid for Research on Health Sciences Focusing on Drug Innovation from The Japan Health Sciences Foundation.

References

1) Anchordoquy T. J., Koe G. S., *J. Pharm. Sci.*, **89**, 289—296 (2000).
2) Lai E., van Zanten J. H., *J. Pharm. Sci.*, **91**, 1225—1232 (2002).
3) Li B., Li S., Tan Y., Stolz D. B., Watkins S. C., Block L. H., Huang L., *J. Pharm. Sci.*, **89**, 355—364 (2000).
4) Anchordoquy T. J., Carpenter J. F., Kroll D. J., *Arch. Biochem. Biophys.*, **348**, 199—206 (1997).
5) Molina M. C., Allison S. D., Anchordoquy T. J., *J. Pharm. Sci.*, **90**, 1455—1455 (2001).
6) Crowe J. H., Leslie S. B., Crowe L. M., *Cryobiology*, **32**, 355—366 (1994).
7) van Winden E. C., Zhang W., Crommelin D. J., *Pharm. Res.*, **14**, 1151—1160 (1997).
8) Hsu C. C., Nguyen H. M., Yeung D. A., Brooks D. A., Koe G. S., Bewley T. A., Pearman R., *Pharm. Res.*, **12**, 69—77 (1995).
9) Horii F., "Solid State NMR of Polymers," Chap. 3, ed. by Ando I., Elsevier, Amsterdam, 1998, pp. 51—81.
10) Andronis V., Zografi G., *Pharm. Res.*, **14**, 410—414 (1997).

Glass Transition-Related Changes in Molecular Mobility below Glass Transition Temperature of Freeze-Dried Formulations, as Measured by Dielectric Spectroscopy and Solid State Nuclear Magnetic Resonance

SUMIE YOSHIOKA, YUKIO ASO

National Institute of Health Sciences, 1-18-1 Kamiyoga, Setagaya-ku, Tokyo 158-8501, Japan

Received 27 April 2004; revised 7 September 2004; accepted 14 September 2004

Published online 29 November 2004 in Wiley InterScience (www.interscience.wiley.com). DOI 10.1002/jps.20244

ABSTRACT: The purpose of this study was to explore why changes in the molecular mobility associated with glass transition, the timescale of which is on the order of 100 s, can be detected by measuring the nuclear magnetic resonance relaxation times that reflect molecular motions on the order of 10 kHz and 1 MHz. The molecular motions in freeze-dried dextran 40k, dextran 1k, isomaltotriose (IMT), and α-glucose comprising a common unit but with different glass transition temperatures, were investigated by dielectric spectroscopy (DES) in the frequency range of 0.01 Hz to 100 kHz and in the temperature range of −20° to 200°C, in order to compare with the molecular motions reflected in nuclear magnetic resonance relaxation times. The α-relaxation process for freeze-dried α-glucose was visualized by DES, whereas those for freeze-dried dextran 40k, dextran 1k, and IMT were too slow to be visualized by DES. The latter freeze-dried cakes exhibited quasi-dc polarization because of proton-hopping–like motion rather than α-relaxation process. The correlation time (τ_c) for the backbone carbon of dextran 40k and IMT, calculated from the measured value of spin-lattice relaxation time in the rotating frame, was found to be close to the relaxation time of proton-hopping–like motion determined by DES (τ_{DES}) at temperatures around glass transition temperature. The timescales of molecular motions reflected in the τ_c and τ_{DES} were significantly smaller than that of motions leading to molecular rearrangement (molecular rearrangement motions), which correspond to α-relaxation. However, the shapes of temperature dependence for the τ_c and τ_{DES} were similar to that of the calorimetrically determined relaxation time of molecular rearrangement motions. Results suggest that the molecular motions reflected in the τ_c and τ_{DES} are linked to molecular rearrangement motions, such that enhancement of molecular rearrangement motions enhances the molecular motions reflected in the τ_c and τ_{DES}. Thus, the τ_{DES} and τ_c can reflect changes in molecular mobility leading to unwanted changes in amorphous formulations, and are thought to be a useful measure for evaluating the stability of formulations. J Pharm Sci 94:275–287, 2005

Keywords: dielectric spectroscopy; solid state NMR; freeze-drying; relaxation time

INTRODUCTION

Amorphous pharmaceuticals, as opposed to crystals, reveal various modes of rotational and diffusive motions leading to molecular rearrangement that may bring about unwanted changes in the system. These motions leading to molecular rearrangement (hereafter referred to as molecular rearrangement motions) exhibit an average relaxation time on the order of 100 s at the calorimetric glass transition temperature (T_g). Furthermore, the average relaxation time

Correspondence to: Sumie Yoshioka (Telephone: 81-3-3700-8547; Fax: 81-3-3707-6950; E-mail: yoshioka@nihs.go.jp)

Journal of Pharmaceutical Sciences, Vol. 94, 275–287 (2005)

changes with changing temperature according to the Adam-Gibbs-Vogel (AGV) and Vogel-Tammann-Fulcher (VTF) equations below and above T_g, respectively.[1]

Investigations of the molecular mobility of freeze-dried formulations containing polymer excipients have demonstrated that glass transition occurs partially even at temperatures below T_g, enhancing molecular rearrangement motions and leading to decreases in the physical and chemical stability.[2–6] Changes in the temperature dependence of molecular rearrangement motions associated with the glass transition have been detected by measuring nuclear magnetic resonance (NMR) relaxation times such as laboratory and rotating frame spin-lattice relaxation times (T_1 and $T_{1\rho}$) and spin–spin relaxation time (T_2) of ^1H and ^{13}C.[7–12] However, there is no clear explanation for the question why changes in the temperature dependence of molecular rearrangement motions with a relaxation time longer than 100 s at sub-T_g can be detected by measuring NMR relaxation times such as T_1, $T_{1\rho}$, and T_2 of ^1H and ^{13}C that reflect molecular motions on the order of 1 MHz, 10 kHz, and >10 kHz, respectively. Thus, the aim of this investigation was to elucidate the relationship between molecular rearrangement motions and molecular motions reflected in NMR relaxation times in freeze-dried formulations containing polymer excipients. In an effort for this purpose, molecular motions reflected in NMR relaxation times were first compared with molecular motions reflected in dielectric spectra, which is capable of observing molecular motions ranging from 0.01 Hz to 100 kHz.

Dielectric relaxation spectroscopy (DRS) is a useful method of determining molecular mobility, as is NMR relaxation measurement. NMR measures the fluctuation of a certain atom, whereas DRS measures the reorientation of a molecular dipole. NMR allows determination of the molecular motion of a specific site in the molecule, whereas DRS reflects the mobility of molecular dipoles that are usually difficult to specify in the case of polymers. The correlation time, which represents the timescale of molecular motion, cannot be determined directly from the NMR relaxation time, because NMR relaxation time depends on the relaxation mechanism. Therefore, it is necessary to understand the relaxation mechanism in order to calculate the correlation time from the observed relaxation time. However, DRS is able to directly detect the timescale of molecular motions ranging from 10^{-11} to 10^3 s.

DRS has been used to determine the molecular mobility of various amorphous pharmaceuticals and excipients.[13–16] The mobility of water coexisting with excipients has also been investigated using DRS.[17–22] Montes and Cavaille[16] used DRS to observe the γ- and β-relaxation of dextran film, which were assigned to the noncooperative motion of local segments and the cooperative motion of main chain segments, respectively, based on the observed activation energy. Noel et al.[14] observed the α-relaxation of amorphous glucose corresponding to molecular rearrangement motions by DRS.

In this investigation, the molecular motions in freeze-dried dextran 40k, dextran 1k, isomaltotriose (IMT), and α-glucose comprising a common unit but with different T_g's, were first investigated by dielectric spectroscopy (DES). Then, the temperature dependence of the relaxation time determined by DES (τ_{DES}) was compared with that of the correlation time determined by NMR relaxation measurements (τ_c), in order to discuss the relationship between the molecular motions detected by DES and NMR. The τ_c for the backbone carbon of freeze-dried IMT was calculated from the $T_{1\rho}$ value measured in this study, and that of freeze-dried dextran 40k was calculated from the $T_{1\rho}$ value reported previously.[11] Furthermore, the τ_c and τ_{DES} were compared with the timescale of molecular rearrangement motions measured calorimetrically, in order to discuss the correlation of molecular rearrangement motions and molecular motions reflected in the τ_c and τ_{DES}.

EXPERIMENTAL

Freeze-Drying

Freeze-dried samples for DES measurement were prepared as follows: each of dextran 40k (D-4133; Sigma Chemical Co.), dextran 1k (00268; Fluka Production GmbH), IMT (I-0381; Sigma Chemical Co.), and α-D-glucose (anhydrous 158968; Aldrich) was dissolved in distilled water (5% w/w). Conversion of α-D-glucose to β-D-glucose during the dissolution was prevented by cooling the solution with ice. Seven hundred microliters of the solutions was frozen in a polypropylene sample tube (17-mm diameter) by immersion in liquid nitrogen for 10 min, and then dried at a vacuum level below 5 Pa for 23.5 h in a lyophilizer (Freezevac C-1; Tozai Tsusho Co., Tokyo). The shelf temperature was between −35° and −30°C for the first 1 h, 20°C for the subsequent 19 h, and 30°C for the last 3.5 h.

Table 1. T_g of Freeze-Dried Cakes Determined using Differential Scanning Calorimetry

	Dry	23% RH	43% RH	60% RH	75% RH
Dextran 40k	230°C		80	58	35
Dextran 1k	167				
IMT	122	53	33	7	
α-Glucose	35				

To prepare freeze-dried samples for $T_{1\rho}$ measurement, 400 μL of IMT solution (2.5% w/w) was frozen in a polypropylene sample tube (10-mm diameter).

Freeze-dried samples with various water contents were obtained by storing the freeze-dried sample at 15°C for 24 h in a desiccator with a saturated solution of potassium acetate [23% relative humidity (RH)], K_2CO_3 $2H_2O$ (43% RH), NaBr $2H_2O$ (60% RH), or NaCl (75% RH). The T_g of samples was determined by differential scanning calorimetry at a scan rate of 20°C/min (2920; TA Instruments, New Castle, DE), and the results are shown in Table 1.

DES

Dielectric measurements were performed with a dielectric analyzer (model 2970; TA Instruments) operating in the frequency range of 0.01 Hz to 100 kHz and in the temperature range of −20° to 200°C. Gold parallel plate electrodes (ceramic parallel plate, 25 mm) were used. Permittivity was measured with and without a thin Teflon sheet (0.2-mm thickness) inserted between the sample and the upper electrode. The Teflon sheet was used to inhibit charge transfer between the electrode and the sample, as reported for measurement of the Maxwell-Wagner process in a heterogeneous dielectric mixture.[18] Teflon was chosen because of the low permittivity and the lack of dielectric dispersion in the temperature and frequency range examined. The observed values of real permittivity (ε′) and imaginary permittivity (ε″) were relative rather than absolute, because the electrode area, which was larger than the sample area, was used for the calculation of permittivity. Therefore, the ratio of ε″ to ε′ (tan δ) was calculated as a parameter independent of the surface area of the sample.

For measurement in the dry state, lyophilized cakes were placed on the lower electrode, and the chamber enclosing the sample was purged with nitrogen gas for 24 h at a constant temperature (120°C for dextran 40k, 100°C for dextran 1k and IMT, and 25°C for α-glucose). A small container of P_2O_5 was introduced into the chamber for measurement of α-glucose samples. After removing moisture, samples were compressed with a force of 500 N, and permittivity was measured at a constant temperature as a function of frequency. Permittivity was also measured at a constant frequency of 1 Hz and 1 kHz as a function of temperature. Heating rate was 5°C/min for dextran 40k, dextran 1k, and IMT, and 20°C/min for α-glucose (rapid measurement to prevent glucose crystallization during the measurement).

Permittivity of the samples containing moisture was measured at 25°C as a function of frequency, immediately after placing the cake (pre-equilibrated at 23%, 43%, 60%, or 75% RH) on the lower electrode (500 N).

Determination of $T_{1\rho}$ by ^{13}C Solid State NMR

The $T_{1\rho}$ of methine carbon in the IMT backbone (Fig. 1) was determined for the peak at 70 ppm (Fig. 2) at temperatures ranging from 5° to 65°C

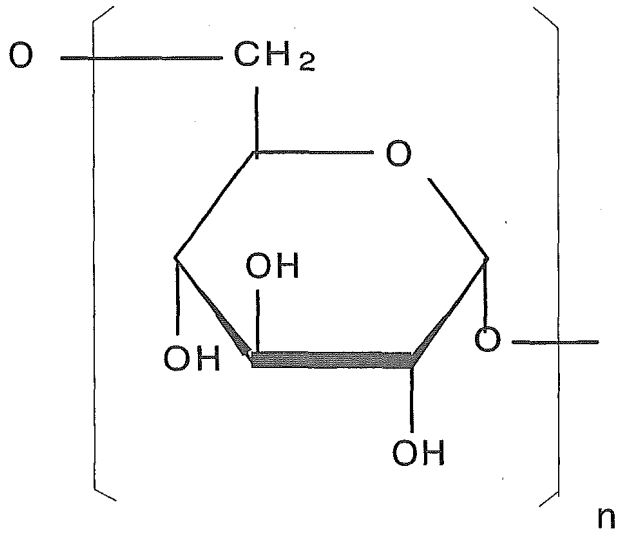

Figure 1. Repeated unit of α-glucose series.

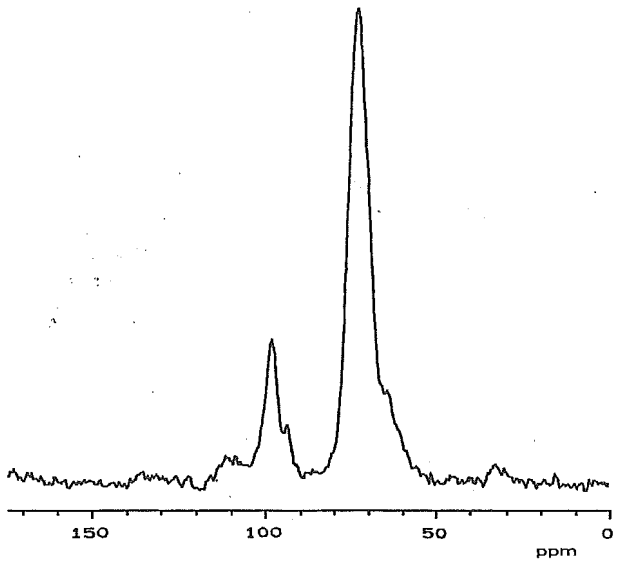

Figure 2. NMR spectrum of lyophilized IMT equilibrated at 43% RH, measured at 25°C and 1 ms of spin-locking duration.

with freeze-dried IMT equilibrated at 43% and 60% RH, using a UNITY plus spectrometer operating at a proton resonance frequency of 400 MHz (Varian Inc., Palo Alto, CA), as previously described.[11] Spin-locking field was equivalent to 57 kHz. The rotor size was 7 mm and spinning speed was 4 kHz. Signal decay was describable with a mono-exponential equation.

RESULTS AND DISCUSSION

Molecular Motions Observed by DES

Figure 3 shows the temperature dependence of the tan δ observed for freeze-dried dextran 40k. The tan δ measured with a Teflon sheet inserted is also shown in Figure 3. The tan δ exhibited a peak around 130°C when measured at 1 Hz with a Teflon sheet inserted (Fig. 3A), but increases in tan δ were only observed in the absence of the Teflon sheet (Fig. 3B). The peak for β-relaxation of dextran 40k is expected to appear below 27°C at 1 kHz, because β-process was observed at 27°C for a film of a larger molecular weight dextran.[16] Therefore, the changes in tan δ observed at 1 kHz (Fig. 3A), the peak of which is expected to appear above 200°C, were attributed to another process that is slower than the β-process.

Figure 4 shows the temperature dependence of tan δ observed at 1 kHz for freeze-dried α-glucose, IMT, and dextran 1k, together with that observed for freeze-dried dextran 40k. Freeze-dried IMT

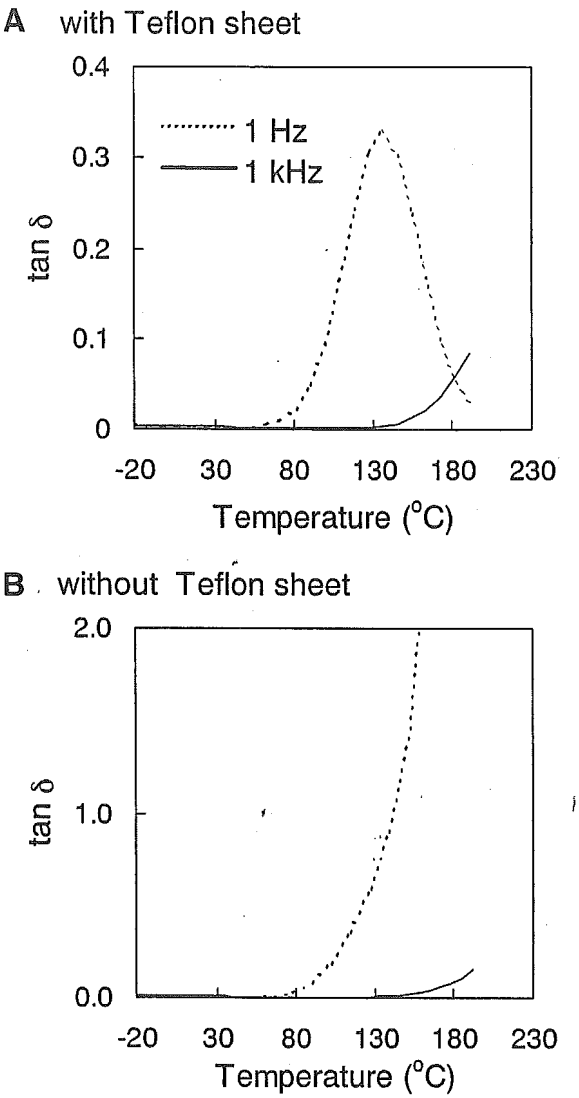

Figure 3. Temperature dependence of tan δ measured for freeze-dried dextran 40k with (A) and without (B) a Teflon sheet at 1 Hz (dashed line) and 1 kHz (solid line).

and dextran 1k exhibited a peak with a Teflon sheet inserted, around 140° and 170°C, respectively (Fig. 4A). This peak was not observed in the absence of the Teflon sheet (Fig. 4B). The increases in tan δ with increasing temperature observed without the Teflon sheet may be attributable to the quasi-dc polarization (referring to low-frequency dispersion accompanied by abnormal increases in permittivity), as reported for hydrated granular or porous solids.[23] This was thought to be because both ε′ and ε″ measured as a function of frequency revealed a substantial increase in the low-frequency region (data not shown). Insertion of a Teflon sheet to inhibit charge transfer into the

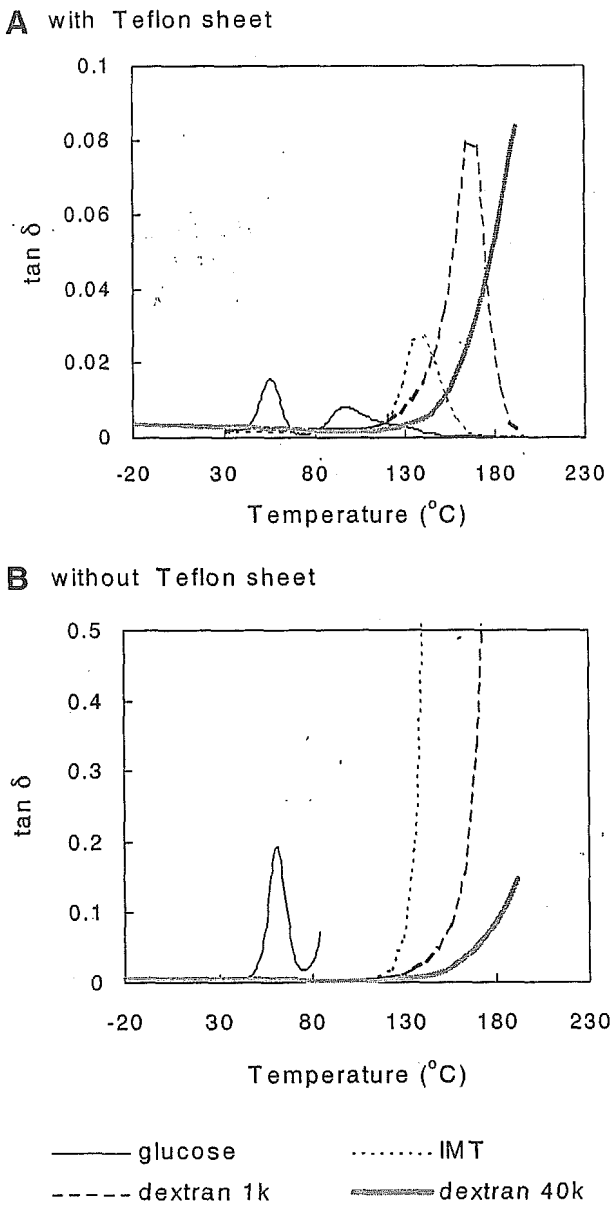

Figure 4. Temperature dependence of tan δ measured for freeze-dried α-glucose, IMT, dextran 1k, and dextran 40k with (A) and without (B) a Teflon sheet at 1 kHz.

electrode enabled the observation of quasi-dc polarization as a peak, in a similar manner as the Maxwell-Wagner process reported for a heterogeneous dielectric mixture.[18]

The mechanism of the observed quasi-dc polarization remains unclear. Quasi-dc polarization has been ascribed to diffusion of ions over the surface of the solid, as reported for hydrated mannitol,[17] or to the proton hopping reported for hydrated proteins.[18,24,25] However, the quasi-dc process observed for freeze-dried α-glucose series cannot be attributed to the hopping of protons in the ionizable carboxylic group as observed in a hydrated protein. A possible explanation for the observed quasi-dc polarization is that a proton-hopping–like process occurs in the hydrogen-bonded network constructed between hydroxy groups in the glucose unit in the form of clusters. However, there still seems to be a question whether such proton-hopping–like process is possible in the nearly dry state.

The frequency at which ε'' shows a maximum value depends on the thickness and permittivity of the sheet used, but can be regarded as a measure for comparing the mean relaxation time of the observed Maxwell-Wagner–like process, namely, proton-hopping–like process. In the freeze-dried IMT, dextran 1k, and dextran 40k, the ε'' value normalized to that observed at the peak (ε''_p) exhibited a similar shape of dielectric spectrum, as shown in Figure 5. The shape of dielectric spectrum did not vary significantly with changing the temperature both below and above the T_g. The dielectric spectra obtained for the freeze-dried IMT showed relatively large scattering.

Freeze-dried α-glucose exhibited two peaks when a Teflon sheet was inserted (Fig. 4A). The peak for tan δ around 100°C was not observed in the absence of the Teflon sheet, in a similar manner as the peaks observed for IMT, dextran 1k, and dextran 40k (Fig. 4B). In contrast, the tan δ peak around 50°C was not affected by the presence of a Teflon sheet. The peak of ε'' corresponding to this tan δ peak was observed only at temperatures above T_g, when measured in the range from 0.01 Hz to 100 kHz, as shown in Figure 6. Furthermore, the distribution of the ε'' peak was larger than that of proton-hopping–like process observed for IMT, dextran 1k, and dextran 40k. These results suggest that the peak observed for tan δ is attributed to α-relaxation—molecular rearrangement motions that are related to the instability of freeze-dried formulations. Noel et al.[14] observed the α-relaxation of α-glucose at 1 kHz and at 70°C, which was higher than the temperature reported herein. This difference in temperature may be attributable to the difference in the water content of the samples.

The other peak observed around 100°C (Fig. 4A) seems to be attributed to a charge transfer process, similar to the proton-hopping–like process observed for IMT, dextran 1k, and dextran 40k, because it was not observed without the Teflon sheet (observed ε' values were negative at temperatures above 85°C) (Fig. 3B). However, the

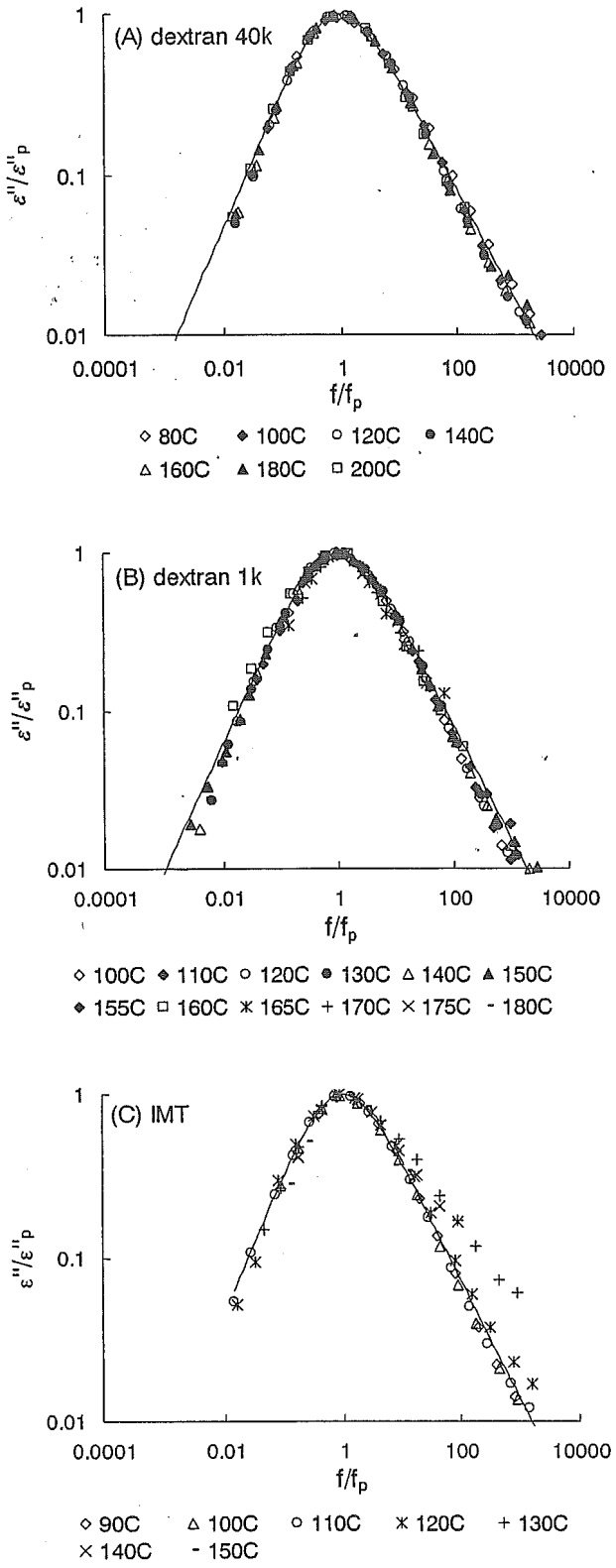

Figure 5. Normalized plot of imaginary permittivity for the Maxwell-Wagner–like process observed in freeze-dried dextran 40k (A), dextran 1k (B) and IMT (C) with a Teflon sheet inserted.

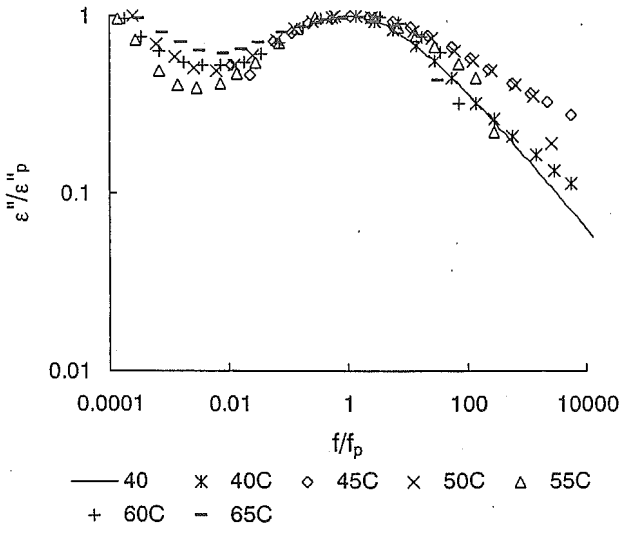

Figure 6. Normalized plot of imaginary permittivity for α-relaxation observed in freeze-dried α-glucose with a Teflon sheet inserted.

mechanism for this charge transfer process may be different from that for the proton-hopping–like process observed for IMT, dextran 1k, and dextran 40k. This was thought to be because this process occurred above T_g, whereas the proton-hopping–like process for IMT, dextran 1k, and dextran 40k occurred below T_g.

Temperature Dependence of Relaxation Time Determined by DES

Figure 7A shows the temperature dependence of the relaxation time of the proton-hopping–like process (τ_{DES}) observed for the freeze-dried dextran 40k, dextran 1k, and IMT, as well as that of the dielectric relaxation time of α-relaxation observed for the freeze-dried α-glucose. Figure 7A also shows the relaxation time of the molecular rearrangement motions in the freeze-dried α-glucose series, calculated from the observed T_g values according to the AGV (solid line) and VTF (dotted line) equations below and above T_g, respectively. The assumption that the fictive temperature (T_f) is equal to T_g (newly formed glass) and the fragility parameter (m) is equal to 70 was made, as reported for amorphous indomethacin.[26] The calculated relaxation time below T_g was not affected by varying the m value from 40 to 100, whereas that above T_g was largely dependent on the m value.[27]

The dielectric relaxation time observed for the freeze-dried α-glucose appeared to reach approximately 100 s at T_g, confirming that α-relaxation is

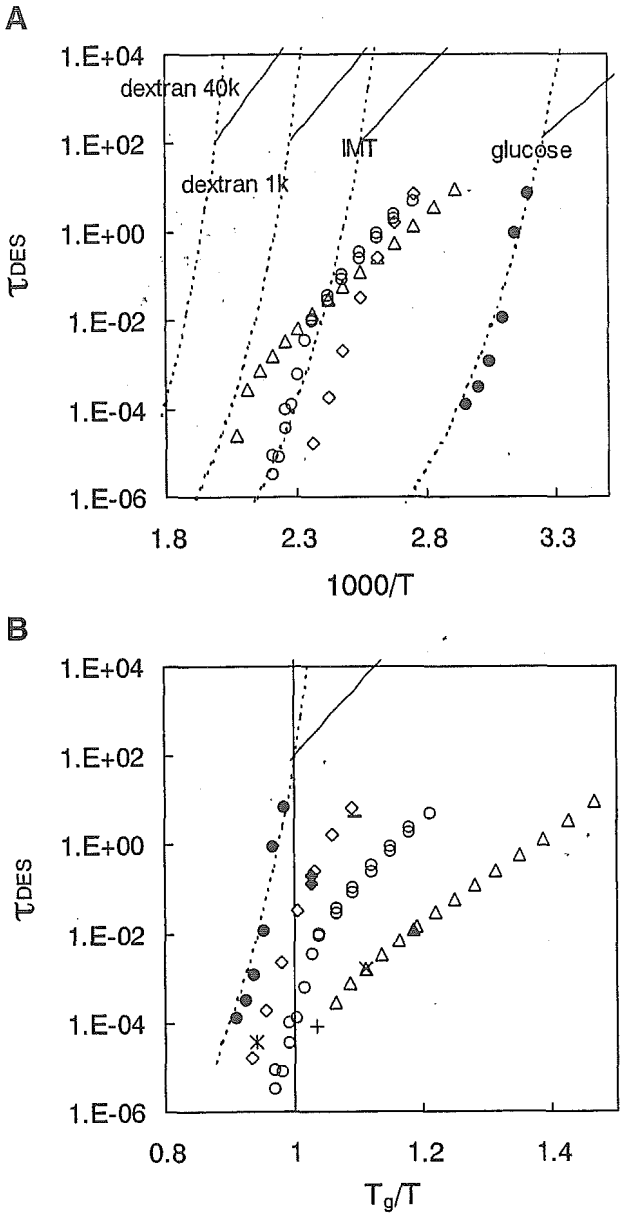

Figure 7. Relaxation time of the proton-hopping–like process observed in freeze-dried dextran 40k (△), dextran 1k (○) and IMT (◇), and that of α-relaxation observed in freeze-dried α-glucose (●) determined with dry samples at various temperatures, plotted against $1000/T$ (A) and T_g/T (B). Solid and dotted lines represent the relaxation time of molecular rearrangement motions calculated according to the AGV and VTF equations, respectively. (B) Also encloses the relaxation time determined with dextran 40k at 25°C and 43% RH (▲), 60% RH (×), and 75% RH (+), and that determined with IMT at 25°C and 23% RH (−), 43% RH (◆), and 60% RH (*).

responsible for this process. This is further supported by the finding that the observed dielectric relaxation time was almost coincident with the relaxation time of molecular rearrangement motions calculated using the VTF equation, although the relaxation time is only an approximation due to the assumed m value.

The τ_{DES} observed for the freeze-dried dextran 40k, dextran 1k, and IMT was shorter than the calculated relaxation time of molecular rearrangement motions (Fig. 7A), indicating that the proton-hopping–like process is faster than molecular rearrangement motions. A plot of the τ_{DES} versus the temperature scaled to T_g in order to conceal the effect of differing T_g values (Fig. 7B), was not in good agreement with the data obtained from different molecular weights. As molecular weight increased, the τ_{DES} at T_g decreased and the difference between the τ_{DES} and the relaxation time of molecular rearrangement motions increased. These results suggest that the rate of the proton-hopping–like process is determined not only by the molecular mobility indicated by the T_g value. If the observed quasi-dc process is assumed to be due to the proton-hopping–like process occurring in clusters constructed between hydroxy groups in the glucose unit as described above, the rate of the process may be affected by the cluster size and distance between clusters, which may depend on the molecular weight. Thus, the difference in molecular weight may result in a difference in the rate of proton-hopping–like process at T_g in addition to a difference in T_g values.

Figure 7B also shows the τ_{DES} observed for freeze-dried dextran 40k and IMT containing moisture. The temperature dependence of the τ_{DES} was not affected by the presence of moisture, and changes in the τ_{DES} were attributable only to changes in T_g. These findings suggest that moisture does not affect the rate of proton-hopping–like process itself, but enhances the process by increasing the molecular mobility as indicated by T_g.

As shown in Figure 7B, the slope of the τ_{DES} versus T_g/T plot increased as the temperature approached T_g from a lower temperature. These changes in temperature dependence were similar to those observed for the relaxation time of molecular rearrangement motions (line in Fig. 7). This similarity in the temperature dependence suggests that the proton-hopping–like process is linked to molecular rearrangement motions such that changes in the temperature dependence of the latter process around T_g result in changes in the

temperature dependence of the former process. Thus, enhancement of molecular rearrangement motions may enhance the proton-hopping–like process. The close relationship between the proton-hopping–like process and molecular rearrangement motions seems to be confirmed by the finding that enhancement in the proton-hopping–like process upon absorption of moisture can be explained only by the decrease in T_g, as described above.

Temperature Dependence of Correlation Time Determined by NMR Relaxation Measurement

Figure 8 shows the temperature dependence of the $T_{1\rho}$ measured for backbone carbon in the freeze-dried IMT. The $T_{1\rho}$ for backbone carbon in the freeze-dried dextran 40k reported previously[11] is also shown in the figure. $T_{1\rho}$ is plotted against $1/T$ in Figure 8A and against the temperature scaled to T_g in Figure 8B. Decreases in $T_{1\rho}$ with increasing temperature were observed for both freeze-dried IMT and dextran 40k even at temperatures below T_g. These shapes of temperature dependence suggest that $T_{1\rho}$ can detect the enhancement of molecular rearrangement motions associated with glass transition partially occurring even at temperatures below T_g.

Correlation time τ_c can be calculated from the observed $T_{1\rho}$ according to eq. (1) if the minimum value of $T_{1\rho}$ is known.[28]

$$\frac{1}{T_{1\rho}} = \frac{A\tau_c}{1+4\omega_1^2\tau_c^2} \qquad (1)$$

where ω_1 is the strength of spin-locking, and $\omega_1^2\tau_c^2$ is equal to 0.5 when $T_{1\rho}$ is the minimum. The change in $T_{1\rho}$ for the freeze-dried IMT equilibrated at 60% RH decreased at high temperatures, and $T_{1\rho}$ appeared to approach the minimum value. The value of A in eq. (1) was calculated assuming that the minimum value of $T_{1\rho}$ can be approximated from the smallest value of $T_{1\rho}$ measured at 60% RH, and used in the calculation of τ_c. Because $T_{1\rho}$ minimum was not observed for freeze-dried dextran 40k even at 75% RH, the value of A for freeze-dried dextran 40k was calculated from the minimum value of $T_{1\rho}$ measured at 86% RH, which had been reported previously.[11] The τ_c value calculated for dextran 40k and IMT is plotted against the temperature scaled to T_g in Figure 9A, and compared with the relaxation time of the proton-hopping–like process (τ_{DES}) in Figure 9B. The relaxation time of molecular rearrangement motions determined

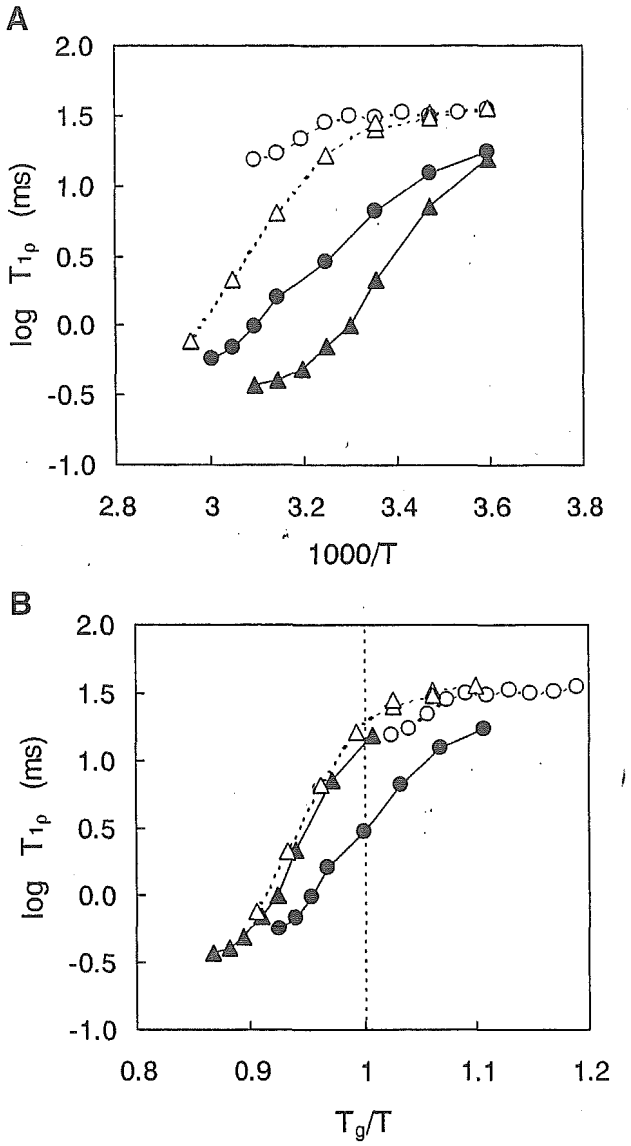

Figure 8. $T_{1\rho}$ of freeze-dried IMT equilibrated at 43% RH (△) and 60% RH (▲), plotted against $1000/T$ (A) and T_g/T (B). $T_{1\rho}$ of freeze-dried dextran 40k at 60% RH (○) and 75% RH (●) reported previously[11] is shown.

calorimetrically is also shown in Figure 9B. The τ_c value derived from $T_{1\rho}$ was shorter than the relaxation time of molecular rearrangement motions for both freeze-dried IMT and dextran 40k.

The $T_{1\rho}$-derived τ_c for the freeze-dried IMT and dextran 40k was on nearly the same order as the τ_{DES} around a T_g/T of 0.95 and 1.06, respectively, and was much smaller than the relaxation time of molecular rearrangement motions determined calorimetrically. As the T_g/T increased above 0.95 and 1.06, the $T_{1\rho}$-derived τ_c for the freeze-dried IMT and dextran 40k, respectively, diverged significantly from the plots for the τ_{DES}. A similar

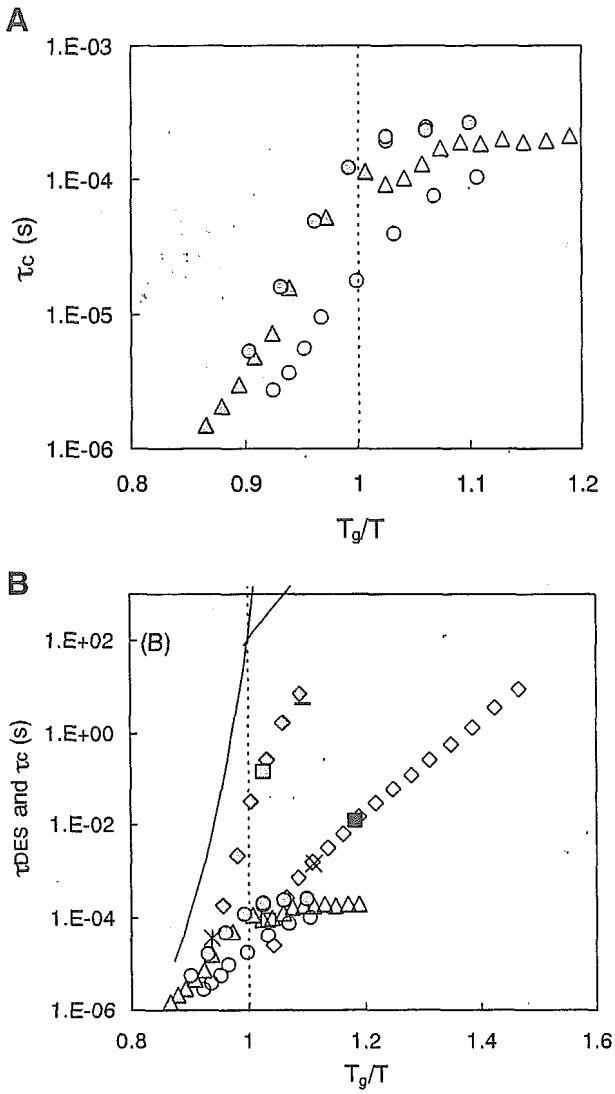

Figure 9. (A) τ_c for the methine carbon of dextran 40k at 60% RH (△), dextran 40k at 75% RH (○), IMT at 43% RH (⊙), and IMT at 60% RH (▲) calculated from the observed value of $T_{1\rho}$. (B) Comparison of the τ_c of methine carbon with the τ_{DES} of the proton-hopping–like process for dextran 40k (◇) and IMT (◈) determined with dry samples at various temperatures, as well as τ_{DES} determined for dextran 40k at 25°C and 43% RH (■), 60% RH (×), 75% RH (+), and τ_{DES} determined for IMT at 25°C and 23% RH (−), 43% RH (▣), and 60% RH (∗). The relaxation time of molecular rearrangement motion determined calorimetrically (solid line) is also shown.

divergence of $T_{1\rho}$-derived τ_c from a DES correlation time at temperatures below T_g has been reported for glucose.[15]

To elucidate the reason for the divergence of the $T_{1\rho}$-derived τ_c from the plots for the τ_{DES}, the τ_{DES} value determined from the dielectric spectrum

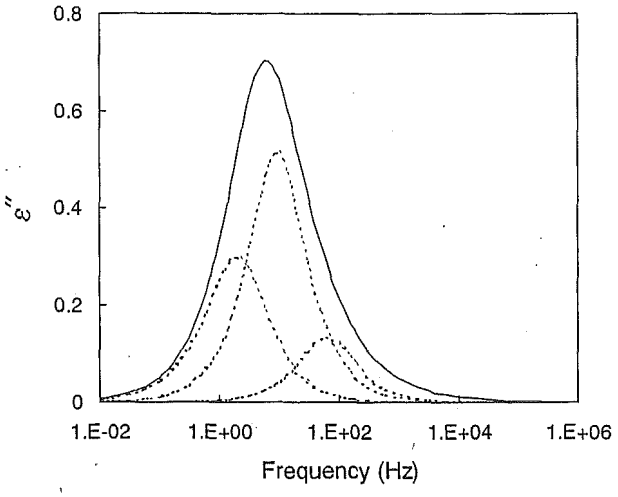

Figure 10. Dielectric relaxation spectrum of freeze-dried IMT at 120°C (solid line). Dashed lines represent three components of the Debye relaxation used for the transformation of τ_{DES} to $T_{1\rho}$.

reflecting the proton-hopping–like process was transformed to the corresponding $T_{1\rho}$ value and compared with the experimentally determined $T_{1\rho}$. The dielectric spectrum obtained for the freeze-dried IMT was first divided into three components of the Debye relaxation, and the three sets of τ and its fraction (f) were then calculated according to eq. (2).[29] An example of the imaginary permittivity (ϵ'') versus frequency plots used for the analysis is shown in Figure 10.

$$\varepsilon'' = \sum_{i=1}^{3} \frac{\Delta\varepsilon_i \omega \tau_i}{1 + \omega^2 \tau_i^2} \qquad (2)$$

$$\text{where } \Delta\varepsilon_i = f_i(\Delta\varepsilon_1 + \Delta\varepsilon_2 + \Delta\varepsilon_3)$$

The three sets of τ and f obtained were used to calculate the spectral density $J(\omega)$ according to eq. (3).[28]

$$J(\omega) = \sum_{i=1}^{3} \frac{f_i \tau_i}{1 + 4\omega^2 \tau_i^2} \qquad (3)$$

Calculated $J(\omega)$ at temperatures ranging from 90° to 150°C are shown as a function of frequency in Figure 11A. Figure 11B shows the temperature dependence of J at 57 kHz, which corresponds to the ω value of the NMR instrument used in this investigation. The value of $T_{1\rho}$ corresponding to the τ_{DES} was calculated from the obtained J according to eq. (4),[28] and the result is shown in Figure 12A.

$$\frac{1}{T_{1\rho}} = AJ = \frac{1 + 4\omega_1^2 \tau_c^2}{T_{1\rho(\min)} \tau_c} J \qquad (4)$$

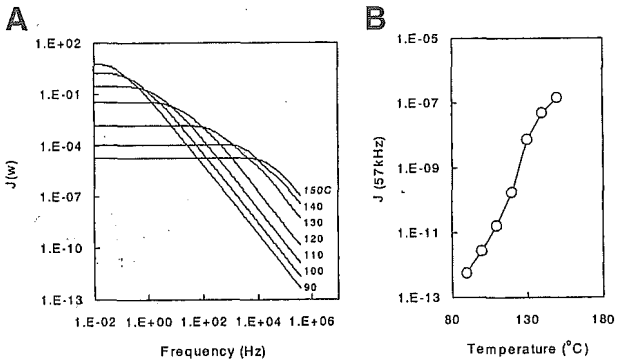

Figure 11. Spectral density calculated from dielectric relaxation spectrum of freeze-dried IMT as a function of frequency (A) and at 57 kHz as a function of temperature (B).

where $\omega^2\tau_c^2$ was assumed to be equal to 0.5. The $T_{1\rho}$ value corresponding to the τ_{DES} for the freeze-dried dextran 40k was calculated from the dielectric spectrum in a similar manner as that of IMT. However, the dielectric spectrum was divided into two rather than three components, because the distribution of the spectrum for dextran 40k was smaller than that for IMT. The value of $T_{1\rho}$ calculated from dielectric spectrum (DES-derived $T_{1\rho}$) is shown in Figure 12B.

Figure 12 encloses the experimentally determined $T_{1\rho}$ value compared with the DES-derived $T_{1\rho}$ value. The measured $T_{1\rho}$ was close to the DES-derived $T_{1\rho}$ around a T_g/T of 0.95 and 1.06 for freeze-dried IMT and dextran 40k, respectively. However, as the T_g/T increased above these values, the measured $T_{1\rho}$ diverged from the DES-derived $T_{1\rho}$ and approached a plateau on the order of 10 ms. This plateau for the measured $T_{1\rho}$ is thought to be due to static spin–spin interactions that affect $T_{1\rho}$. Namely, $T_{1\rho}$ is determined predominantly by static factors rather than by molecular mobility at lower temperatures,[30] at which molecular mobility is very low. As temperature increases above a certain point, the contribution of molecular mobility to $T_{1\rho}$ increases to a degree comparable to static spin–spin interactions, and begins to decrease the measured value of $T_{1\rho}$. The critical temperature at which the increase in molecular mobility begins to be reflected in $T_{1\rho}$ is considered to be the T_{mc} defined previously as the T_g determined by the NMR relaxation time.[9] For freeze-dried dextran 40k, the T_g/T value of 1.06 was close to that of 1.07 calculated for a sample with a T_g of 58°C and a T_{mc} of 35°C (60% RH), and to that of 1.05 calculated for a sample with a T_g of 35°C and a T_{mc} of 20°C

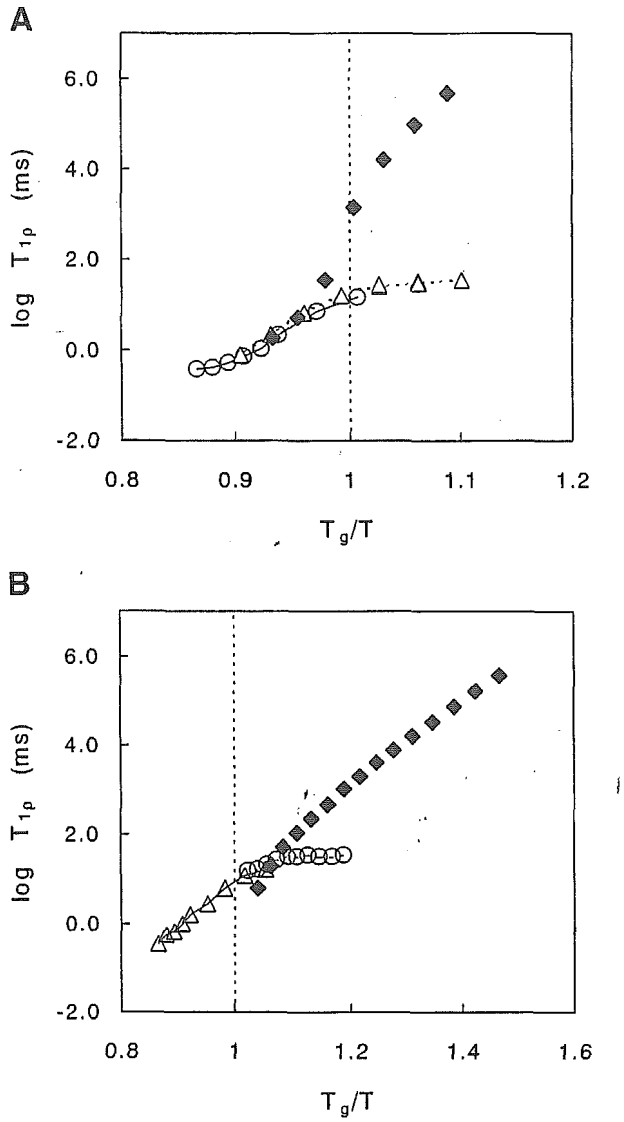

Figure 12. $T_{1\rho}$ observed at 43% RH (△) and 60% RH (○) for freeze-dried IMT (A) and that at 60% RH (○) and 75% RH (△) for freeze-dried dextran 40k (B), compared with $T_{1\rho}$ estimated based on the spectral density calculated from dielectric spectrum (◆).

(75% RH). These findings suggest that $T_{1\rho}$ cannot reflect molecular mobility at temperatures below T_{mc}.

In contrast to the freeze-dried dextran 40k, freeze-dried IMT exhibited a DES-derived $T_{1\rho}$ much larger than the measured $T_{1\rho}$ even at temperatures around T_g, at which $T_{1\rho}$ is expected to reflect molecular mobility. This difference between IMT and dextran 40k suggests that a decrease in molecular weight decreases the rate of the proton-hopping–like process. Thus, even at T_g, the timescale of the proton-hopping–like process

in freeze-dried IMT may become on the order larger than 10 ms, at which $T_{1\rho}$ cannot reflect the rate of process.

Molecular motions in freeze-dried IMT and dextran 40k were too slow to be reflected in $T_{1\rho}$ at temperatures well below T_g such that the measured $T_{1\rho}$ diverged significantly from the DES-derived $T_{1\rho}$ (Fig. 12). However, the coincidence of the measured $T_{1\rho}$ and the DES-derived $T_{1\rho}$ around a T_g/T of 0.95 and 1.06 (although the range is very small) suggests that the timescale of molecular motion reflected in $T_{1\rho}$ is on the same order as that of the proton-hopping–like process. As shown in Figure 7, the τ_{DES} decreased rapidly as temperature approached T_g, showing a similar shape of temperature dependence to that of molecular rearrangement motions. The $T_{1\rho}$-derived τ_c also showed a similar shape of temperature dependence (Fig. 9). The similarity of the temperature-dependence patterns suggests that the molecular motions reflected in $T_{1\rho}$ are linked to molecular rearrangement motions, such that enhancement of molecular rearrangement motions enhances the molecular motions reflected in $T_{1\rho}$. Such linkage was also observed between molecular rearrangement motions and molecular motion reflected in τ_{DES}, as described above (Fig. 7). Fujiwara and Nagayama[31] reported that the exact correlation functions expressed by multiexponential decay observed in the NMR relaxation of macromolecules were well approximated by a single exponential decay. This seems to support the interpretation that molecular rearrangement motions are linked to the molecular motions reflected in $T_{1\rho}$ and τ_{DES}. Because of this linkage between molecular motions, changes in the temperature dependence of molecular rearrangement motions related to the instability of amorphous formulations may be detected by measurement of $T_{1\rho}$ and τ_{DES}.

$T_{1\rho}$ of ^{13}C in the polymer backbone was used as a measure of molecular mobility in the present investigation. However, previous investigations have demonstrated that changes in the temperature dependence for molecular rearrangement motions of freeze-dried dextran can be detected by the T_1 of ^{13}C in the polymer backbone,[10] as well as the T_1 and $T_{1\rho}$ of ^1H.[11] Figure 13 compares the temperature dependence of $T_{1\rho}$ of ^{13}C in the dextran backbone described in this article with those of T_1 of ^{13}C, and T_1 and $T_{1\rho}$ of ^1H reported previously. A change in the slope of the NMR relaxation time versus $1/T$ plot was clearly shown around T_{mc} indicated by arrows. Thus, the shape of

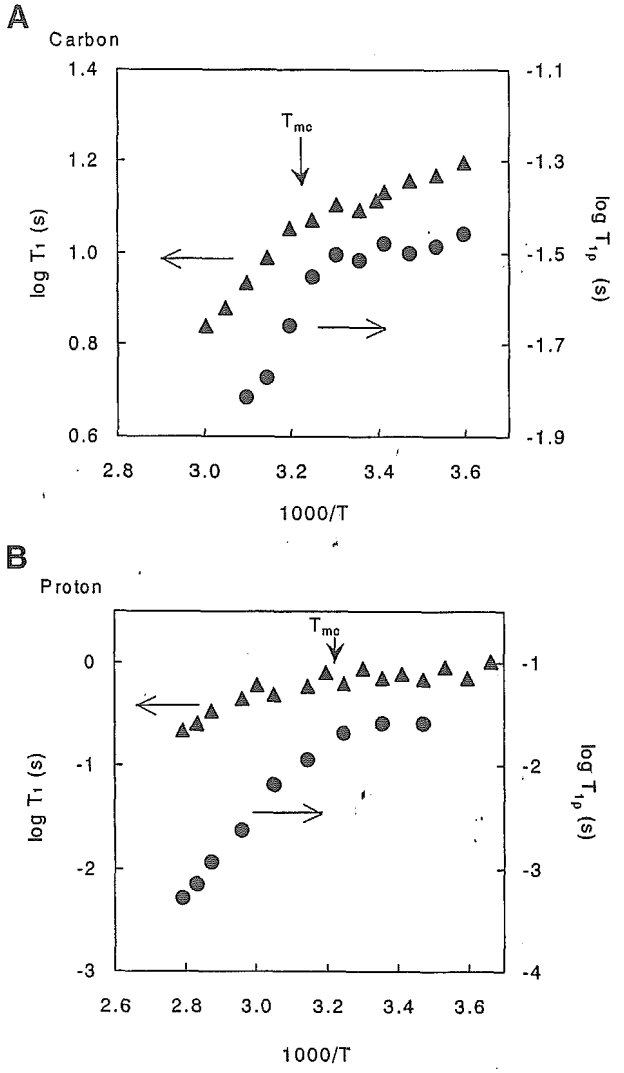

Figure 13. Temperature dependence of T_1 (▲) and $T_{1\rho}$ (●) of methine carbon (A) and proton (B) in the freeze-dried dextran 40k observed at 60% RH.

temperature dependence of T_1, which reflects a smaller timescale of molecular motions than $T_{1\rho}$, was similar to that of $T_{1\rho}$. This finding suggests that molecular motion with a smaller timescale than the molecular motion reflected in $T_{1\rho}$ is also linked to molecular rearrangement motions.

CONCLUSIONS

DES was able to detect molecular rearrangement motions in freeze-dried α-glucose. However, molecular rearrangement motions in freeze-dried dextran 40k, dextran 1k, and IMT were too slow to be observed by DES from 0.01 Hz to 100 kHz,

and proton-hopping–like process rather than molecular rearrangement motions was reflected in the dielectric spectra. The τ_c for the backbone carbon of dextran 40k and IMT, calculated from the observed $T_{1\rho}$ value, was found to be close to the relaxation time of proton-hopping–like process (τ_{DES}) at temperatures around T_g. The timescales for molecular motions reflected in the τ_c and τ_{DES} were significantly smaller than that for molecular rearrangement motions, but the shapes of temperature dependence for the τ_c and τ_{DES} were similar to that of the relaxation time of molecular rearrangement motions. This suggests that molecular motions reflected in the τ_{DES} and the τ_c are linked to molecular rearrangement motions. Because of this linkage between molecular motions, changes in the temperature dependence of molecular rearrangement motions related to the instability of amorphous formulations may be detected by measurement of $T_{1\rho}$ and τ_{DES}.

This thought seems to address the question why changes in molecular rearrangement motions with a relaxation time longer than 100 s at sub-T_g can be detected by measuring NMR relaxation times that reflect molecular motions on the order of 10 kHz and 1 MHz.

REFERENCES

1. Shamblin SL, Tang X, Chang L, Hancock BC, Pikal MJ. 1999. Characterization of the time scales of molecular motion in pharmaceutically important glasses. J Phys Chem 103:4113–4121.
2. Yoshioka S, Aso Y, Kojima S. 2000. Temperature dependence of bimolecular reactions associated with molecular mobility in lyophilized formulations. Pharm Res 17:925–929.
3. Yoshioka S, Aso Y, Kojima S. 2004. Temperature- and glass transition temperature-dependence of bimolecular reaction rates in lyophilized formulations described by the Adam-Gibbs-Vogel equation. J Pharm Sci 93:1062–1069.
4. Aso Y, Yoshioka S, Kojima S. 2004. Molecular mobility-based prediction of the crystallization rate of amorphous nifedipine and phenobarbital in PVP solid dispersions. J Pharm Sci 93:384–391.
5. Yoshioka S, Aso Y, Nakai Y, Kojima S. 1998. Effect of high molecular mobility of poly(vinyl alcohol) on protein stability of lyophilized γ-globulin formulations. J Pharm Sci 87:147–151.
6. Yoshioka S, Tajima S, Aso Y, Kojima S. 2003. Inactivation and aggregation of β-galactosidase in lyophilized formulation described by Kohlrausch-Williams-Watts stretched exponential function. Pharm Res 20:1655–1660.
7. Kalichevsky MT, Jaroszkiewicz EM, Ablett S, Blanshard JMV, Lillford PJ. 1992. The glass transition of amylopectin measured by DSC, DMTA and NMR. Carbohydr Polym 18:77–88.
8. Kalichevsky MT, Jaroszkiewicz EM, Blanshard JMV. 1993. A study of the glass transition of amylopectin-sugar mixtures. Polymer 34:346–358.
9. Yoshioka S, Aso Y, Kojima S. 1999. The Effect of excipients on the molecular mobility of lyophilized formulations, as measured by glass transition temperature and NMR relaxation-based critical mobility temperature. Pharm Res 16:135–140.
10. Yoshioka S, Aso Y, Kojima S, Sakurai S, Fujiwara T, Akutsu H. 1999. Molecular mobility of protein in lyophilized formulations linked to the molecular mobility of polymer excipients, as determined by high resolution ^{13}C solid-state NMR. Pharm Res 16:1621–1625.
11. Yoshioka S, Aso Y, Kojima S. 2002. Different molecular motions in lyophilized protein formulations as determined by laboratory and rotating frame spin-lattice relaxation times. J Pharm Sci 91:2203–2210.
12. Yoshioka S, Aso Y, Kojima S. 2003. Mobility of lyophilized poly(vinylpyrrolidone) and methylcellulose as determined by the laboratory and rotating frame spin-lattice relaxation times of ^{1}H and ^{13}C. Chem Pharm Bull 51:1289–1292.
13. Andronis V, Zografi G. 1998. The molecular mobility of supercooled amorphous indomethacin as a function of temperature and relative humidity. Pharm Res 15:835–842.
14. Noel TR, Parker R, Ring SG. 2000. Effect of molecular structure and water content on the dielectric relaxation behaviour of amorphous low molecular weight carbohydrates above and below their glass transition. Carbohydr Res 329:839–845.
15. Moran GR, Jeffrey KR, Thomas JM, Stevens JR. 2000. A dielectric analysis of liquid and glassy solid glucose/water solutions. Carbohydr Res 328: 573–584.
16. Montes H, Cavaille JY. 1999. Secondary dielectric relaxations in dried amorphous cellulose and dextran. Polymer 40:2649–2657.
17. Derbyshire H, Feldman Y, Bland CR, Broadhead J, Smith G. 2002. A study of the molecular properties of water in hydrated mannitol. J Pharm Sci 91: 1080–1088.
18. Suherman PM, Taylor PM, Smith G. 2002. Development of a remote electrode system for monitoring the water content of materials inside a glass vial. Pharm Res 19:337–344.
19. Jain SK, Johari GP. 1988. Dielectric studies of molecular motions in the glassy states of pure and aqueous poly(vinylpyrrolidone). J Phys Chem 92: 5851–5854.